Analysis of Drag on Elliptic Cylinders in Tandem Arrangement

Author

ASIF ANWAR

Regn. Number

NUST201463099MSMME62014F

Supervisor

DR. EMAD UDDIN

DEPARTMENT OF DESIGN AND MANUFACTURING ENGINEERING

SCHOOL OF MECHANICAL & MANUFACTURING ENGINEERING

NATIONAL UNIVERSITY OF SCIENCES & TECHNOLOGY

ISLAMABAD

AUGUST 2018

Analysis of Drag on Elliptic Cylinders in Tandem Arrangement

Author

ASIF ANWAR

Regn. Number

NUST201463099MSMME62014F

A thesis submitted in partial fulfillment of the requirements for the degree of

MS Design and Manufacturing Engineering

Thesis Supervisor:

DR. EMAD UDDIN

Thesis Supervisor's Signature: _____

DEPARTMENT OF DESIGN AND MANUFACTURING ENGINEERING

SCHOOL OF MECHANICAL & MANUFACTURING ENGINEERING

NATIONAL UNIVERSITY OF SCIENCES & TECHNOLOGY

ISLAMABAD

AUGUST 2018

National University of Sciences & Technology

MASTER THESIS WORK

We hereby recommend that the dissertation prepared under our supervision by

<u>ASIF ANWAR</u> Reg No. <u>NUST201463099MSMME62014F</u>

Titled: <u>"Analysis of Drag on Elliptic Cylinders in Tandem Arrangement"</u> be accepted in partial fulfillment of the requirements for the award of Masters in Mechanical Engineering degree with (Grade) _____

<u>Examination Committee Members</u>

1. Dr. Zaib Ali   Signature: _____

2. Dr. Sami Ur Rahman   Signature: _____

3. Dr. Mushtaq Khan   Signature: _____

Supervisor's name: Dr. Emad Uddin   Signature: _____

                                                    Date: _____

Head of Department _____   Date _____

<u>COUNTERSIGNED</u>

                                    _____

Date: _____   Dean/Principal

Thesis Acceptance Certificate

Certified that final copy of MS/MPhil thesis written by **Mr. Asif Anwar** (Regn. Number **NUST201463099MSMME62014F**) of **SMME** has been vetted by undersigned, found complete in all respects as per NUST Statues/Regulations, is free of plagiarism, errors, and mistakes and is accepted as partial fulfillment for award of MS/MPhil Degree. It is further certified that necessary amendments as pointed out by GEC members of the scholar have also been incorporated in the said thesis.

Signature _____

Name of Supervisor **Dr. Emad Uddin**

Date _____

Signature (HOD) _____

Date _____

Signature (Principal) _____

Date _____

Declaration

I certify that this research work titled "*Analysis of Drag on Elliptic Cylinders in Tandem Arrangement*" is my own work. The work has not been presented elsewhere for assessment. The material that has been used from other sources it has been properly acknowledged / referred.

Signature of Student

ASIF ANWAR

NUST201463099MSMME62014F

Plagiarism Certificate (Turnitin Report)

This thesis has been checked for Plagiarism. Turnitin report endorsed by Supervisor is attached.

Signature of Student

ASIF ANWAR

Signature of Supervisor

Copyright Statement

Dedicated to my beloved Parents and all well-wishers who remained

faithful and trust-worthy during this time

Acknowledgements

I would like to express my sincere gratitude to my advisor **Dr. Emad Uddin** for the continuous support during my project and related research, for his patience, motivation, and immense knowledge. His guidance helped me in all the time of research and writing of this thesis.

I would like to acknowledge the help and support provided by Dr. Zaib Ali, Dr. Sami Ur Rahman, Dr. Mushtaq Khan, Dr. Muhammad Safdar, Dr. Syed Omer Gilani, Dr. Ali Zaidi, and Dr. Jawad Aslam. I greatly appreciate and heartfelt thanks for their great contribution in completion of this work.

I am also very thankful to Mr. Mujahid Saeed, Mr. Sameed and Mr. Asfand for their support.

Abstract

From literature it is observed that only a few studies are focused on prediction of integral flow parameters on flow around elliptic cylinders. To best of author's knowledge there are no studies reported on combined effects of Angle of Incidence (A.O.A), Axis Ratio (e), Size Ratio (S.R), Center-to-Center Distance (S) and Reynold's Number (R_e). I have attempted to experimentally measure the effect of integral parameters on Drag Coefficient of elliptic cylinders in tandem arrangement. The A.O.A is varied as 0°, 30°, 60°. A.R and S.R is varied at two points 0.5 and 1.0 only. The R_e was varied at two points 7000 and 14000.

Key Words: Elliptic Cylinder, Reynold's Number, Tandem Arrangement, Angle of Incidence, Axis Ratio, Size Ratio, Center-to-Center Distance

Table of Contents

List of Figures

Chapter 1: Introduction

Water tunnel is a setup which is used to study the hydrodynamic nature of objects submerged in water. The working principle of water tunnel is similar to wind tunnel but working fluid is different. Wind tunnel is replaced by water tunnel to find various forces, for e.g, lift, drag and pressure etc. Other helpful applications of water tunnel are flow visualization and PIV calculations because of its simplicity of use. For the flow with low Reynold Number, oil is a good substitute instead of water. Test bodies and models used in water tunnel can be manufactured quickly and at low cost.

1.1. Background

Flow around spheres and circular cylinders have been object of interest since the early days of fluid dynamics. Research has been done by many researchers in this area and review papers have also been written. However, the elliptic cylinders have not been thoroughly investigated and there is a lot to be done in understanding the flow around elliptic cylinders.

1.2. Scope of Work

The aim of this work is to measure the drag coefficient on elliptic cylinders of Size Ratio 0.5 and 1.0 using water tunnel.

1.3. Methodology

In this research, elliptic cylinders of Size Ratio 0.5 & 1.0 were 3D printed using PLA and connected to two load cells. Load cells were calibrated using standard weights and connected to HX711 amplifier and Arduino UNO microcontroller. The results of drag on elliptic cylinders were displayed in serial monitor.

Chapter 2: Literature Review

The most studied problem in fluid mechanics is flow around the bluff bodies. A bluff body is the one in which length in flow direction is close to or equal to length perpendicular to the flow direction. The bluff bodies cause large flow separation. Strouhal Number (S_t), Coefficient of Lift (C_L), Coefficient of Drag (C_d) and other integral flow parameters and functional relationships among these parameters are the main outcomes of these studies [28]. Circular cylinders placed in different arrangements in the flow field have been subject of various studies because it is of paramount importance in engineering applications which aim to prevent accidents and disaster. In fluid dynamics the flow around circular cylinder is of paramount importance [15]. This is not only because the flow interference of two circular cylinders is the root cause of wake induced vibrations but it also rudimentary in comprehending the flow around multiple cylinders [4]. Comprehensive reviews on flows around two circular cylinders and wake induced vibrations were presented by [32], [33], [34]. Cylindrical structures in arrays are frequently seen in engineering applications. Typical examples include offshore structures, marine risers, group of chimney stacks, tubes in heat exchangers, bridge piers, stays, masts, chemical reaction towers and closely separated skyscrapers. The fluid forces and predominant vortex frequencies are the major considerations in design of engineering structures. Both steady and un-steady fluid forces acting on the structures are linked to the characteristics of the flow structure. The alternate vortex shedding from the upstream structures impinging on the downstream structures may cause large fluctuating pressure on the downstream structure, leading to structural vibrations, acoustic noise, resonance and ultimately structural failure. Numerous failures in practical applications of cylindrical structures in cross flow are illustrated in [5], [6], [21], [22], [23], [24] and [3]. Structural failures can easily cost from a million to billions of dollars. So it is of paramount importance to comprehend the fluid behavior related with multiple cylindrical structures in cross flow [35].

Boundary Layers formation and separation can be observed for the fluid flowing around bluff body. Boundary layers remain attached upto certain Reynold Number, also known as critical Reynold Number. After the critical Reynold Number boundary layers start to get separated from the top and bottom of the bluff. This phenomenon is called vortex shedding. Downstream the body, vortex shedding leads to formation of primary von Karman Vortex street. Primary von Karman Vortex Street is initially stable, becomes unstable as the vortex street moves along the downstream of the body and eventually breaks down at large downstream distance. [29] provided rationale for this phenomena by arguing that the vortex street break down occurred because of variation in the mean velocity profile. According to [10] at R_e 150, break down of primary Karman vortex occurred at 70~100D. The vortices have ability to arrange themselves again and form the secondary von Karman vortex street. [1], [7], [20] enquired the secondary wake patterns of flat plate and circular cylinder. Coefficient of drag (C_d), Strouhal Number (S_t) and other

parameters of flow and the functional relation between them is also effected by change in shedding pattern [28].

Flow past missiles, submarines, rotor blades and wing can be more closely approximated as flow past the elliptic cylinders rather than circular cylinders [16]. In modern engineering applications the circular shapes are falling out of preference and elliptic shapes are gaining more and more acceptance because the offer lesser resistance to flow. [14] arrived at conclusion that elliptic pipes in his heat exchanger offered lower resistance to flow. Parameters such as Major and Minor Axis Length, Angle of Attack and Axis Ratio etc had impact on flow behavior [28].An elliptic cylinder with A.R 1 is circular because the major and minor axis lengths are equal.

Numerous authors analyzed flow behavior around an elliptic cylinder mounted at an angle to incoming flow, experimentally [8], [30], [31] and numerically [2], [11], [17], [18], [19], [25], [27]. None of these analysis focused on integral flow parameters. However, main focus of these analysis was initial flow development. Some of these analyses also determined the effect of angle of incidence on the circulation and movement of separation points on the surface.

Spectral element method was used by [12], [13] to study flow around elliptic cylinders. Parameter space graph was plotted and various vortex shedding regimes were pointed out. In recent past [9[found out the impact of A.R by varying it from 0.3 to 1 and keeping Angle of Incidence constant at zero for the Reynold Number 40. The important findings of this study were that at A.R > 0.6, the pressure forces dominated and at A.R<0.6, the viscous forces dominated.

Chapter 3: Experimental Setup

Water tunnel used for this experiment uses FlowPak horizontal type centrifugal pump of 3 Cuses Capacity, 15 feet total Head, 1450 rpm speed and 10 Pump Horse Power. A Variable Frequency Drive (VFD) controller was used to control pump speed and hence the resulting flow.

3.1. Ultrasonic Flow Meter

The flow measurements were taken at pump discharge pipe, as shown, using ChronoFLO 430 Ultrasonic Flow Meter. These flow measurements were used to calculate water speed at pump discharge pipe for various frequencies. It was found that pump is capable of producing flow speeds of 0.13768 m/s at 15 Hz and 0.45000 m/s at 50 Hz. For this experimental study frequency of 20 Hz was selected for which the corresponding flow velocity is 0.18840 m/s.

Figure 3.1.1: Ultrasonic Flow Meter Display

Figure 3.1.2: Transducers installed on discharge pipe

3.2. 3D-Printer

Anycubic Kossel 3-D Printer, used Poly Lactic Acid (PLA) plastic for 3D printing of 4 Elliptic cylinders. Printing speed was 30mm/s and printing temperature was 2100C. Layer height, shell thickness and fill density were 0.2mm, 0.8mm and 50% respectively. 2 elliptic cylinders of Major Axis (a) 75mm and Minor Axis (b) 37.5mm were printed and 2 other elliptic cylinders of Major Axis (a) 37.5mm and Minor Axis (b) 18.75mm were printed. However, two circular cylinders of ɸ 37.5mm made of Stainless Steel were used for validation.
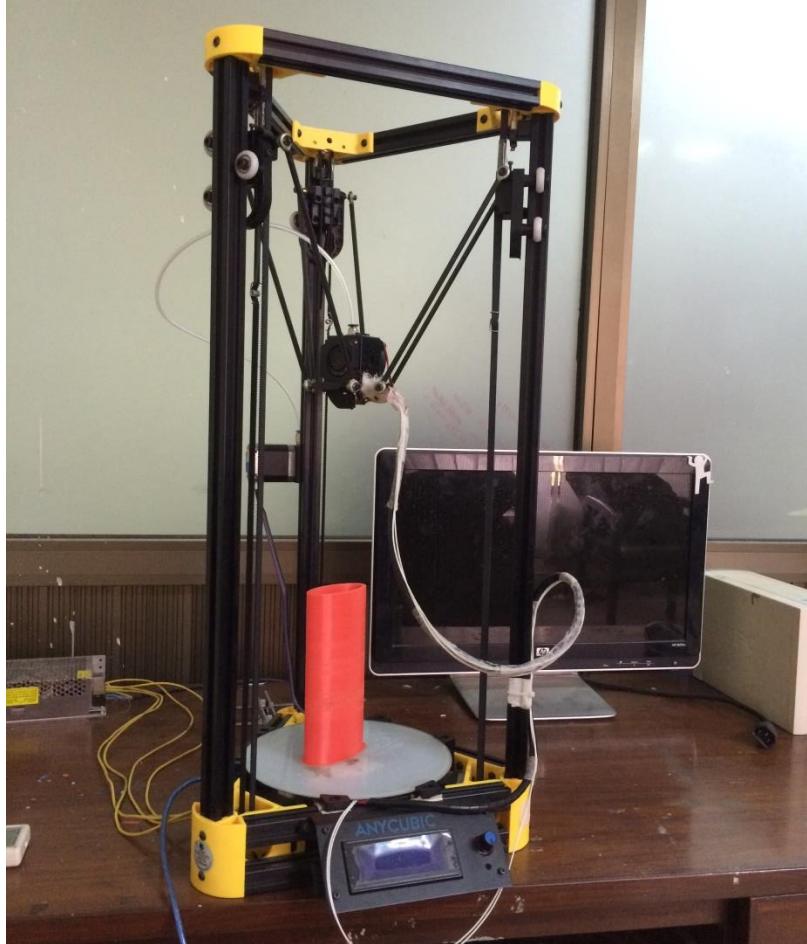
Figure 3.2.1: Printing of elliptic cylinders with Anycubic 3 D Printer

3.3. Load Cell, Amplifier & Microcontroller

2 Bar Type Load Cells of 1kg in conjunction with HX-711 amplifier and Arduino UNO microcontroller are employed for drag measurement. The load cells are based on strain gauges. The electrical resistance of these strain gauges changes with change in applied force/pressure. The signal from the load cell is weak, so an HX-711 Amplifier is employed to amplify the signal coming from strain gauge/load cell. The signal from HX-711 goes to microcontroller Arduino UNO which is connected to laptop as shown. The calibration program written in Arduino Integrated Development Environment (IDE) software is uploaded to Arduino UNO micro-controller. The results in grams are shown in a serial monitor. The load cell is calibrated using standard weights.

 The four wires coming from load cell are connected in following order to HX-711:

Excitation+ (E+) or VCC is red

Excitation- (E-) or ground is black

Output+ (O+), Signal+ (S+) or Amplifier+ (A+) is white

O-, S- or A- is green or blue

And VDD, VCC, DAT, CLK and GND from HX-711 are connected to respective pins on Arduino UNO
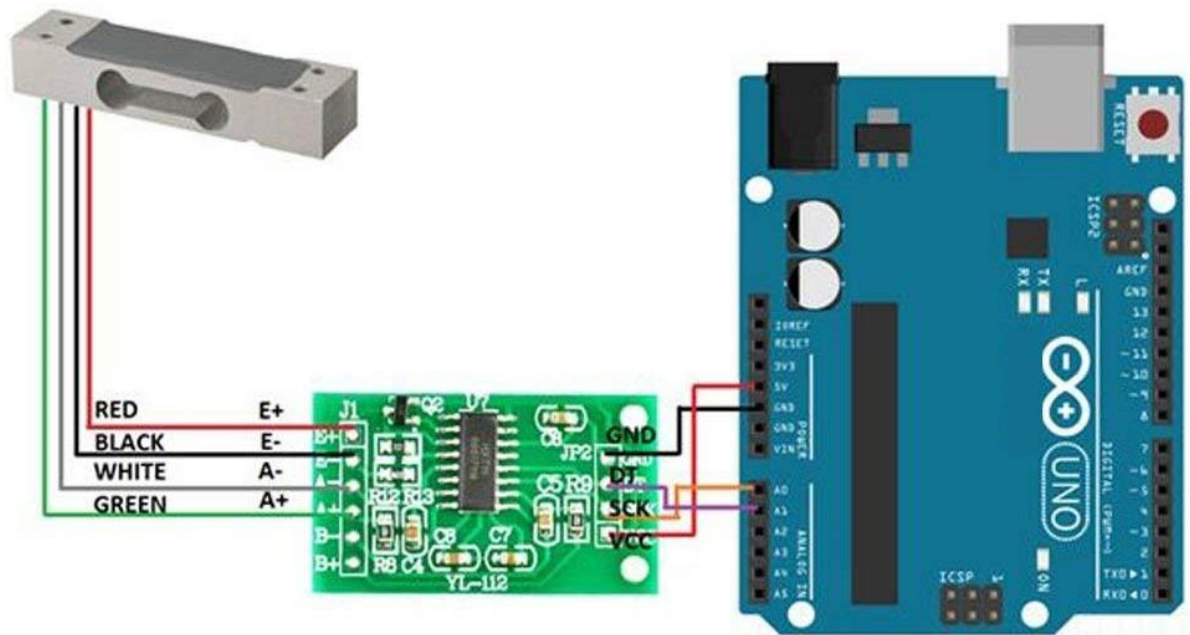
Figure 3.3.1: Load Cell, HX711 and Arduino UNO wiring diagram

3.4. Procedure

Cylinders were mounted on test frame in tandem arrangement as shown in Figure. R_e was kept 7000 for elliptic cylinders with Major Axis 37.5mm & Minor Axis 18.75mm.Whereas R_e was 14000 for elliptic cylinders with Major Axis 75mm and Minor Axis 37.5mm. Comparison with literature was performed at R_e 7000 with circular cylinder of Ø 37.5mm. The center-to-center distance (S) was varied from twice the Major Axis length to six times. Axis Ratio (e=b/a) was 0.5 for elliptic cylinders and 1 for circular cylinders. Size Ratio (a $_{Downstream\ Cylinder}$ / a $_{Upstream\ Cylinder}$) was 0.5 and 1 for the experimental setups. Orientation (α) was varied from 0° (when elliptic cylinder's major axis (a) was parallel to the flow) to 60°. Moreover, orientation of

7

upstream and downstream cylinders was same for any given setup. Table of experimental setups used is given below.

Figure 3.4.1: CAD Model of cylinder mounting assembly

Figure 3.4.2: CAD Model of Water Tunnel

Figure 3.4.3: Experimental Arrangement of cylinders

Fig. 3.4.4: Elliptic Cylinders in Water Tunnel

Fig 3.4.5: Center-to-Center Distance between elliptic cylinders in tandem arrangement

Table 1 Experimental Setups Used

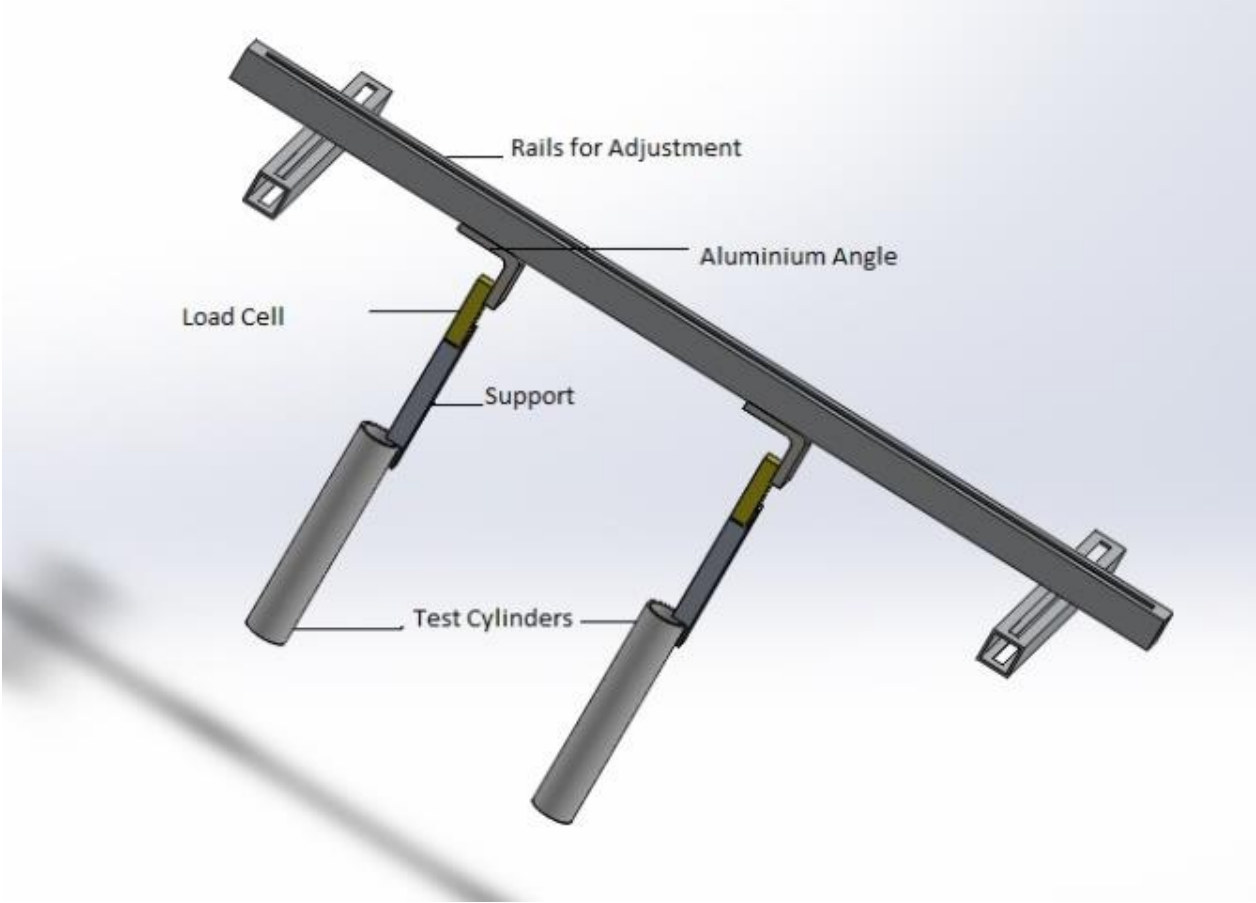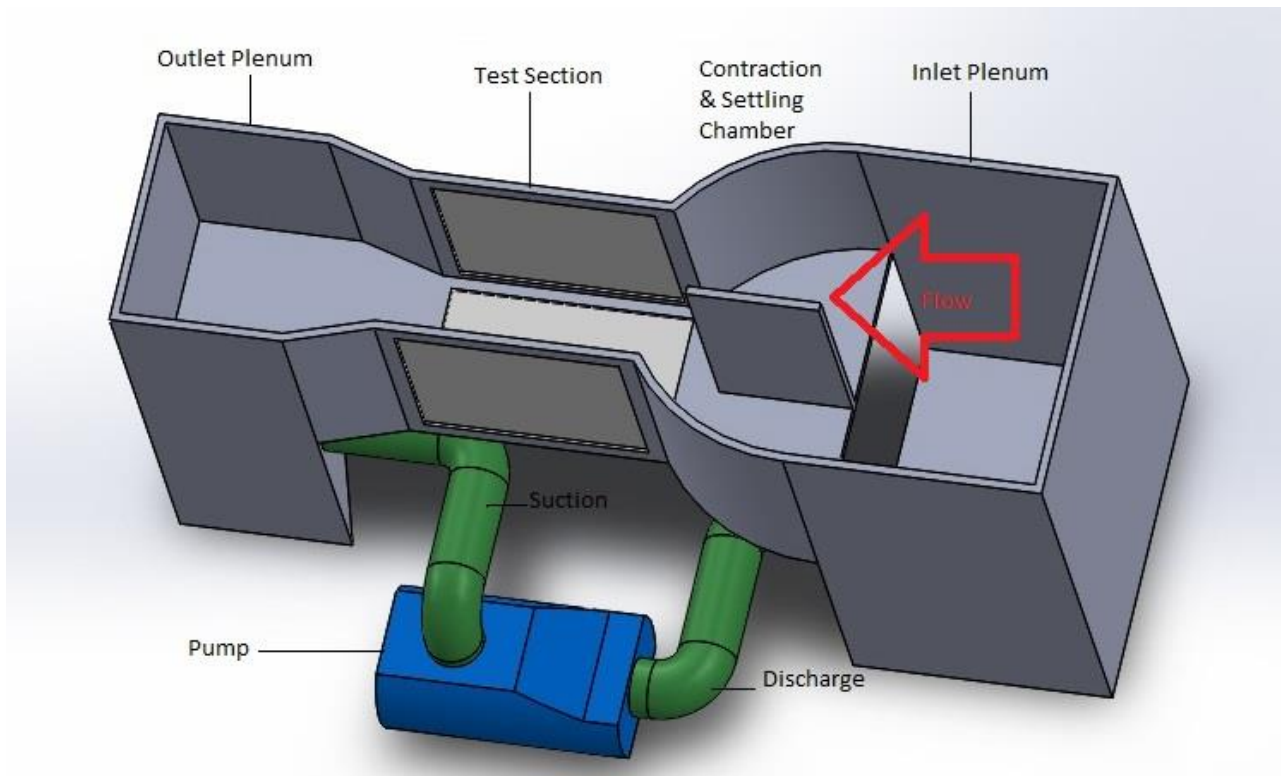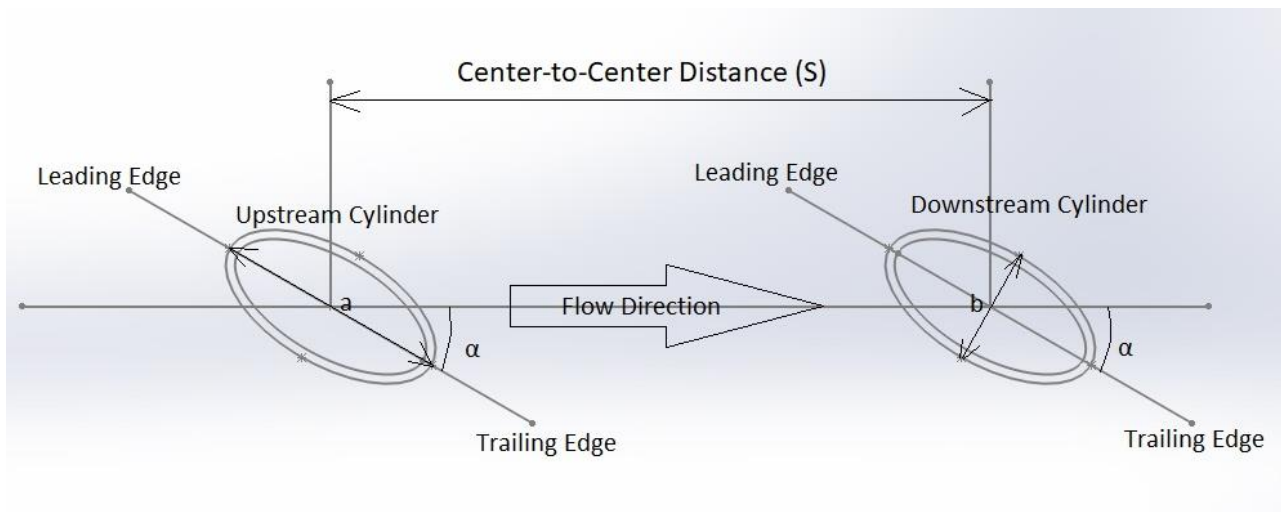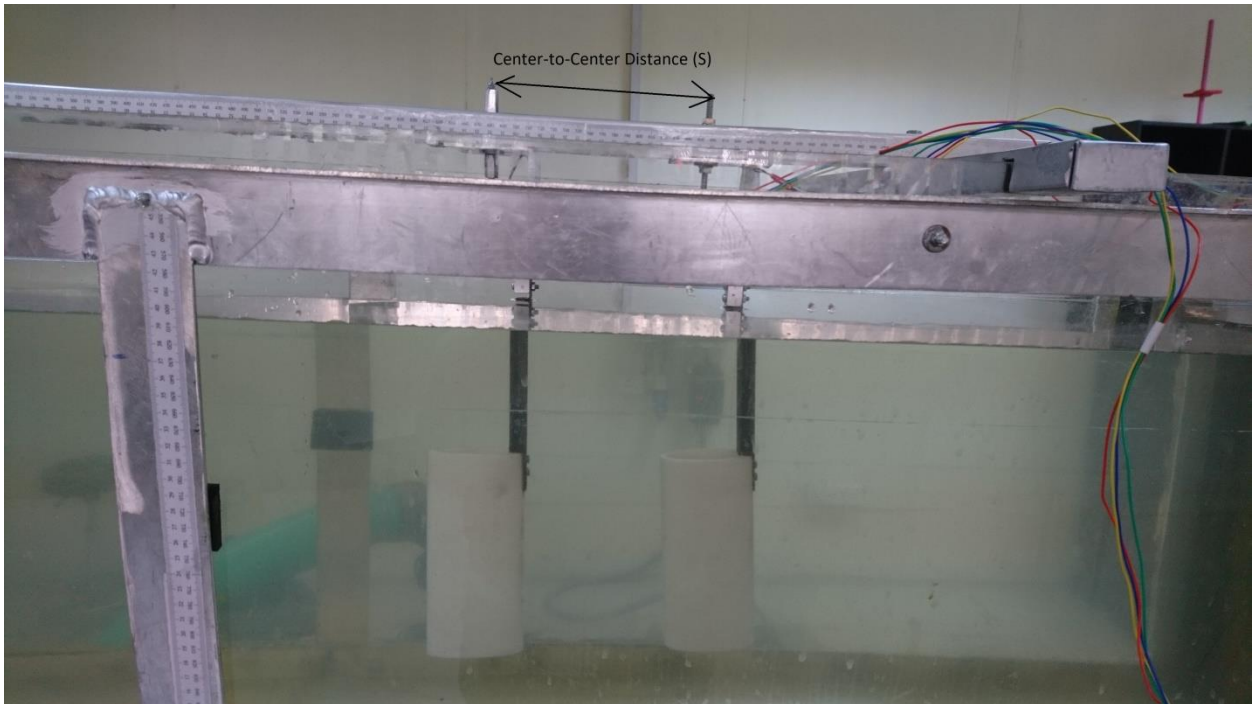| Exp #	Upstream Cylinder	Downstream Cylinder	α (Degrees)	Center-to-Center Spacing (S)	Axis Ratio (A.R)	Size Ratio ($a_{Downstream}$ / $a_{Upstream}$)	Reynold No. (R_e)
1	$\emptyset$ = 37.5mm	$\emptyset$ = 37.5mm	0	2	1	1	7,000
2	$\emptyset$ = 37.5mm	$\emptyset$ = 37.5mm	0	4	1	1	7,000
3	$\emptyset$ = 37.5mm	$\emptyset$ = 37.5mm	0	6	1	1	7,000
4	a = 75mm; b=37.5mm	a = 75mm; b=37.5mm	0	2	0.5	1	14,000
5	a = 75mm; b=37.5mm	a = 75mm; b=37.5mm	30	2	0.5	1	14,000
6	a = 75mm; b=37.5mm	a = 75mm; b=37.5mm	60	2	0.5	1	14,000
7	a = 75mm; b=37.5mm	a = 75mm; b=37.5mm	0	4	0.5	1	14,000
8	a = 75mm; b=37.5mm	a = 75mm; b=37.5mm	30	4	0.5	1	14,000
9	a = 75mm; b=37.5mm	a = 75mm; b=37.5mm	60	4	0.5	1	14,000
10	a = 75mm; b=37.5mm	a = 75mm; b=37.5mm	0	6	0.5	1	14,000
11	a = 75mm; b=37.5mm	a = 75mm; b=37.5mm	30	6	0.5	1	14,000
12	a = 75mm; b=37.5mm	a = 75mm; b=37.5mm	60	6	0.5	1	14,000
13	a = 75mm; b=37.5mm	a=37.5mm, b=18.75mm	0	2	0.5	0.5	14,000
14	a = 75mm; b=37.5mm	a=37.5mm, b=18.75mm	30	2	0.5	0.5	14,000
15	a = 75mm; b=37.5mm	a=37.5mm, b=18.75mm	60	2	0.5	0.5	14,000
16	a = 75mm; b=37.5mm	a=37.5mm, b=18.75mm	0	4	0.5	0.5	14,000
17	a = 75mm; b=37.5mm	a=37.5mm, b=18.75mm	30	4	0.5	0.5	14,000
18	a = 75mm; b=37.5mm	a=37.5mm, b=18.75mm	60	4	0.5	0.5	14,000
19	a = 75mm; b=37.5mm	a=37.5mm, b=18.75mm	0	6	0.5	0.5	14,000
20	a = 75mm; b=37.5mm	a=37.5mm, b=18.75mm	30	6	0.5	0.5	14,000
21	a = 75mm; b=37.5mm	a=37.5mm, b=18.75mm	60	6	0.5	0.5	14,000
22	a = 37.5mm; b=18.75mm	a = 37.5mm; b=18.75mm	0	2	0.5	1	7,000
23	a = 37.5mm; b=18.75mm	a = 37.5mm; b=18.75mm	30	2	0.5	1	7,000
24	a = 37.5mm; b=18.75mm	a = 37.5mm; b=18.75mm	60	2	0.5	1	7,000
25	a = 37.5mm; b=18.75mm	a = 37.5mm; b=18.75mm	0	4	0.5	1	7,000
26	a = 37.5mm; b=18.75mm	a = 37.5mm; b=18.75mm	30	4	0.5	1	7,000
27	a = 37.5mm; b=18.75mm	a = 37.5mm; b=18.75mm	60	4	0.5	1	7,000
28	a = 37.5mm; b=18.75mm	a = 37.5mm; b=18.75mm	0	6	0.5	1	7,000
29	a = 37.5mm; b=18.75mm	a = 37.5mm; b=18.75mm	30	6	0.5	1	7,000
30	a = 37.5mm; b=18.75mm	a = 37.5mm; b=18.75mm	60	6	0.5	1	7,000

Chapter 4: Comparison of experimental results with literature

4.1. Results of Experiments 1 ~ 3

3 Experiments were performed at R_e **7000** with circular cylinders of A.R 1.0, S.R 1.0 and results were compared with the results in literature. Our experimental results showed strong relation with the results in literature. Alam and Meyer, 2011 performed these experiments at R_e **55,000**. For Upstream cylinder, as the center-to-center distance (S) is increased from 2 to 6, C_d initially decreases, then again increases. For Downstream cylinder, as the center-to-center distance increases from 2 to 6, C_d gradually increases from negative to positive value. And comparison of both is shown in Figures 1 and 2.
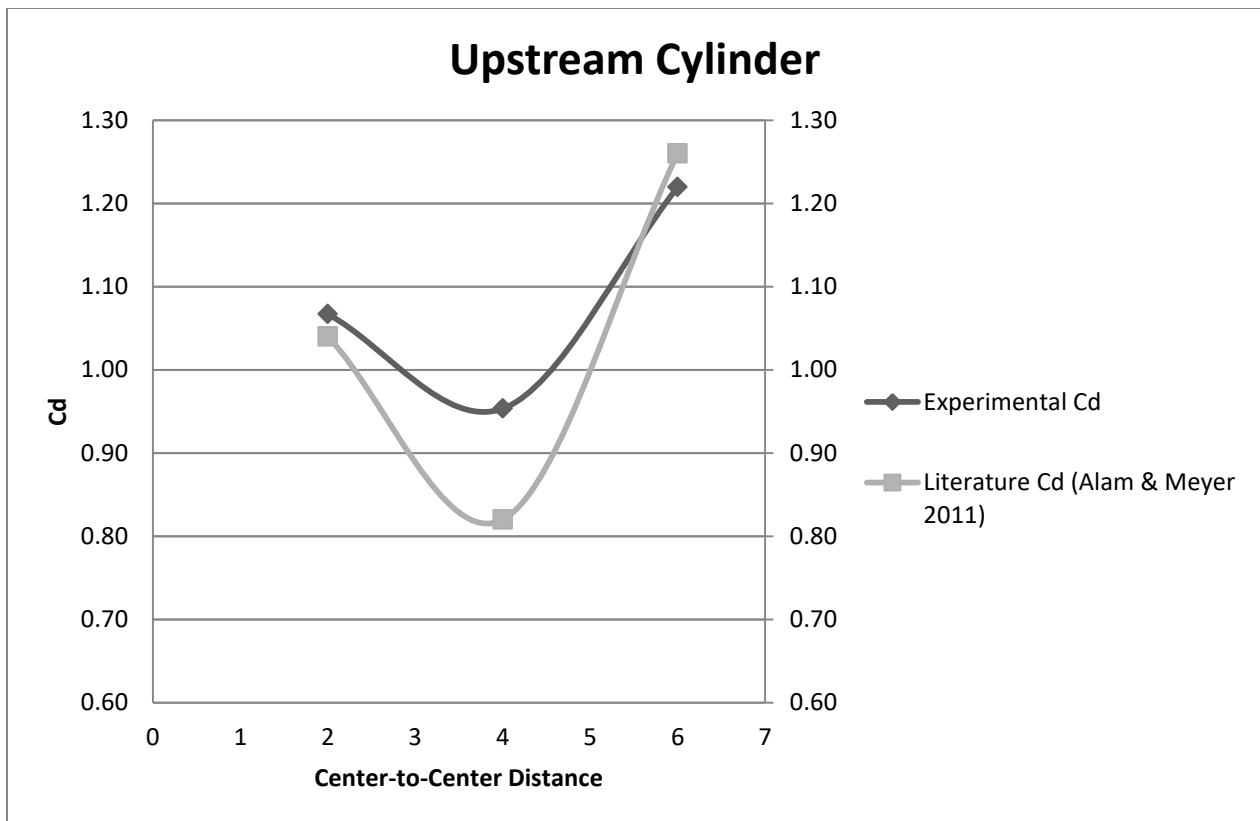
Figure 4.1.1: Comparison of experimental C_d with literature C_d for Upstream circular cylinder Ø 37.5mm
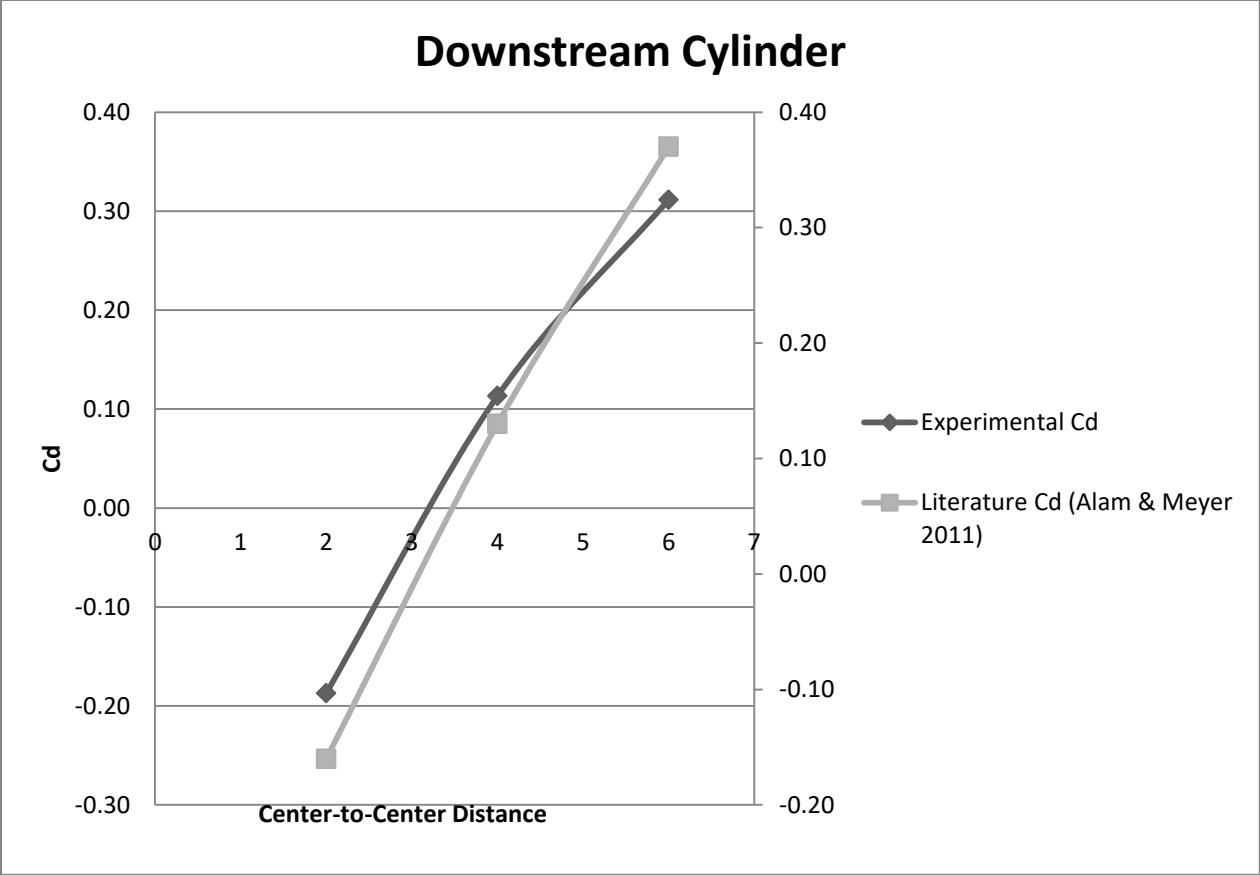
Figure 4.1.2: Comparison of experimental C_d with literature C_d for Downstream circular cylinder Ø 37.5mm

Chapter 5: Results and Conclusions

5.1. Results of Experiments 4 ~ 12

9 experiments were performed at R_e **14000** and following parameters were used for cylinders. Upstream elliptic cylinder a= 75mm, b= 37.5mm, A.R= 0.5, **S.R= 1.0** and downstream elliptic cylinder a= 75mm, b= 37.5mm, A.R=0.5.

Figure 5.1.1.a: Experimental C_d Upstream Cylinder a= 75mm, b= 37.5mm, A.R= 0.5 & S.R=1.0	**Figure 5.1.1.b:** Numerical C_d Upstream Cylinder a= 75mm, b= 37.5mm, A.R= 0.5 & S.R=1.0
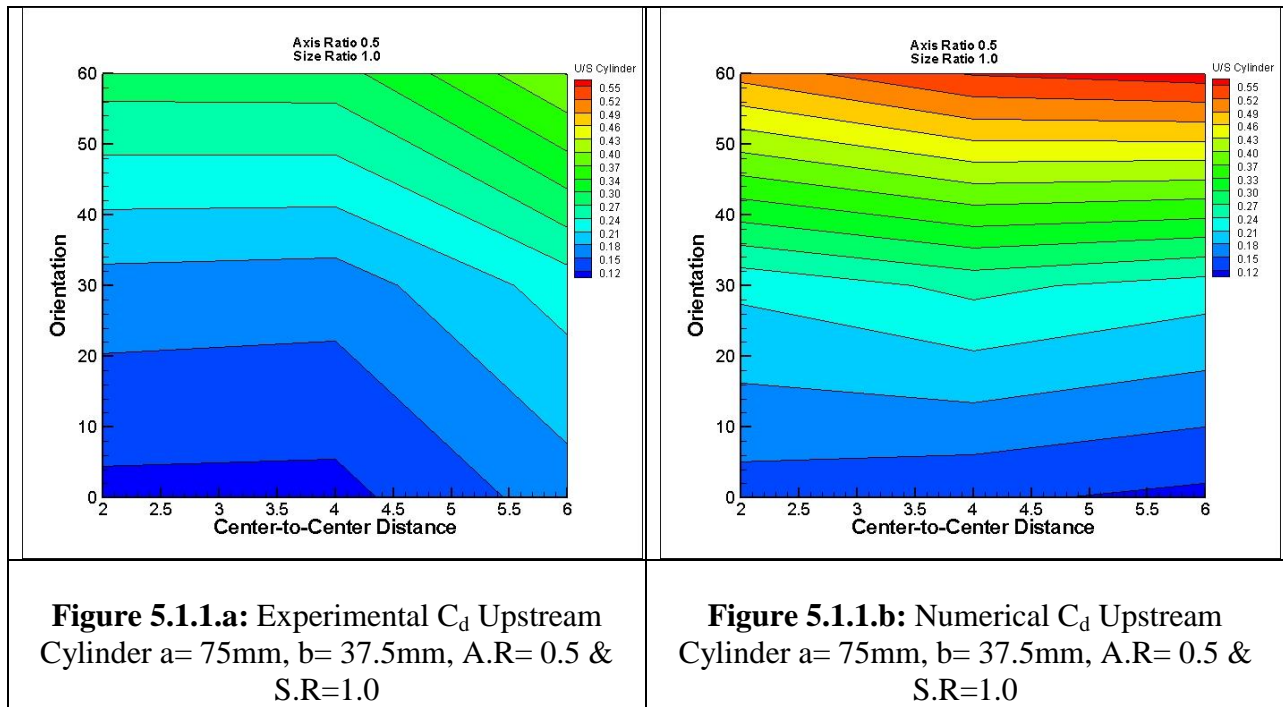
Coefficient of drag (C_d) increases with an increase in the center-to-center distance (S) and orientation for both experimental and numerical studies. This increase is from 0.12 to 0.40 for experimental study and 0.15 to 0.55 for numerical study.

Also it is evident from the experimental study that as center-to-center distance (S) increases beyond 4 and orientation increases beyond 30° drag consistently increases.

Figure 5.1.2.a: Experimental C_d Downstream Cylinder a= 75mm, b= 37.5mm, A.R= 0.5 & S.R=1.0	Figure 5.1.2.b:Numerical C_d Downstream Cylinder a= 75mm, b= 37.5mm, A.R= 0.5 & S.R=1.0
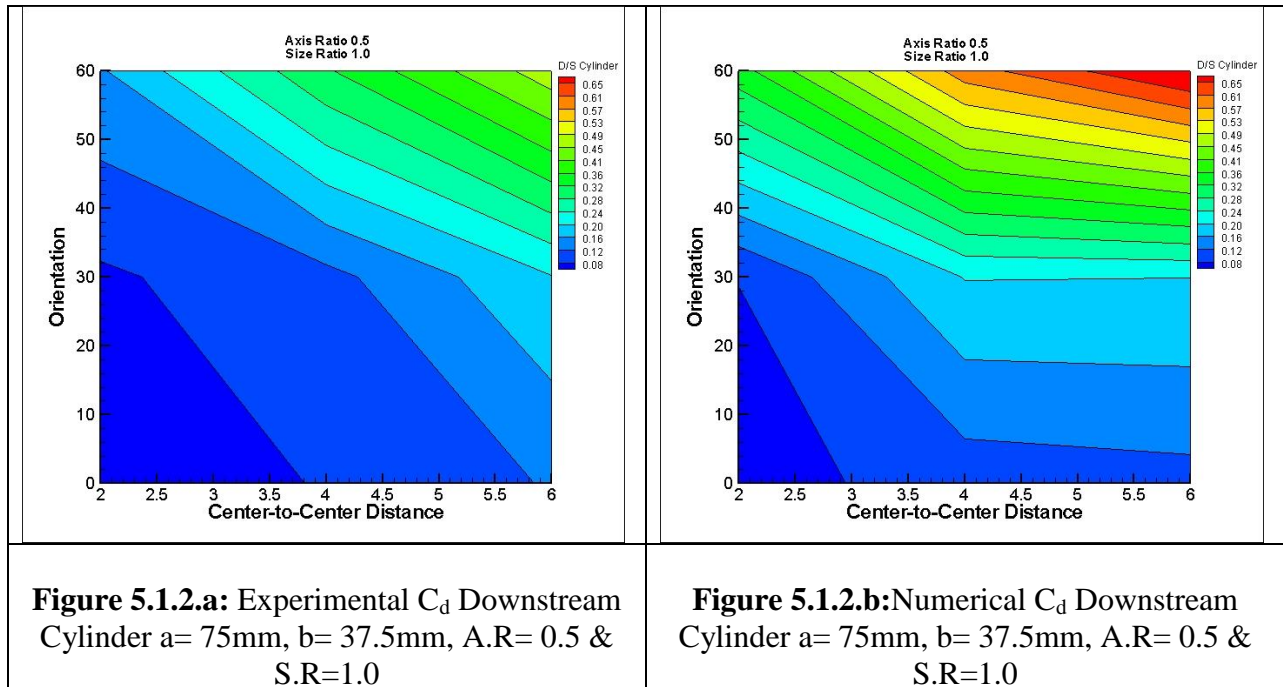
Coefficient of drag (C_d) increase from 0.08 ~ 0.16 when the center-to-center distance (S) increases from 2 to 6 in both experimental and numerical study.

Coefficient of drag (C_d) also increases with increase of orientation (α). This effect is more enhanced for higher orientation and higher center-to-center distance (S). Maximum drag 0.49 and 0.65 is experienced at 60° orientation (α) and 6 center-to-center distance (S) for experimental and numerical studies respectively.

Figure 5.1.3.a: α=0°; S=4; A.R=0.5; S.R=1.0

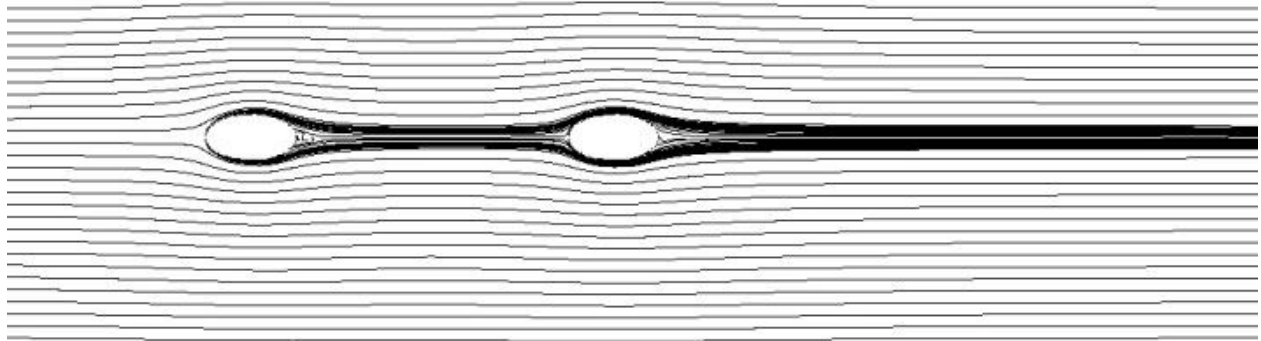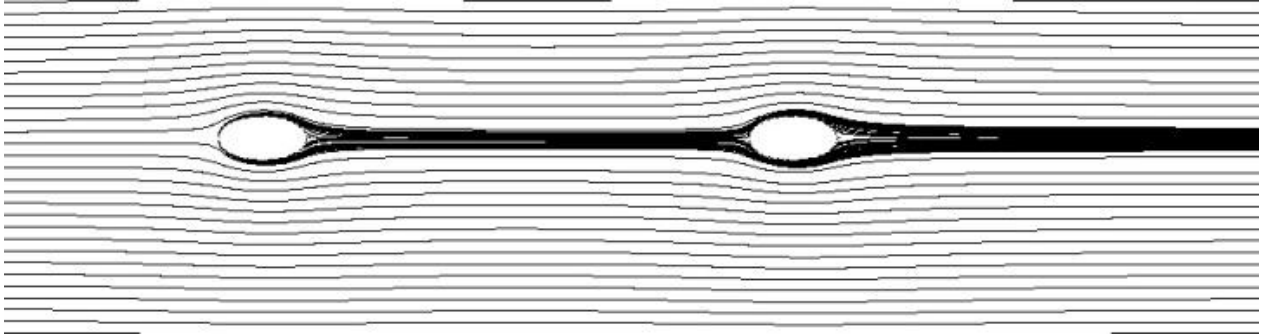**Figure 5.1.3.b:** α=0°; S=6; A.R=0.5; S.R=1.0

At α=0°, S=4 and S=6 streamlines clearly show boundary layer separation as the fluid flows around upstream elliptic cylinders. Shear layers get detached from both upstream cylinders at S=4 and 6. Therefore the pressure at back stagnation point is lower than the pressure at front stagnation point. This low pressure causes drag on upstream cylinders. The wake width at narrowest point of wake is 16% greater for S=4 as compared to S=6. The greater wake width causes lower drag. So the drag at S=4 is lower than at S=6. This can also be seen from surface plots of upstream cylinder. Now for downstream cylinder, the recirculation wake can be ascribed as the high pressure region in front of downstream cylinder and low pressure region behind the upstream cylinder. Shear layers separation is clearly visible at trailing edge of downstream cylinders as well. Therefore the pressure at back stagnation point is lower than the pressure at front stagnation point. This low pressure cause drag on downstream cylinders. Moreover, the greater wake width which impinges on downstream cylinders cause lower drag. So the drag at S=4 is lower than at S=6. This is also clear from surface plots of downstream cylinders.

Figure 5.1.4.a: α=30°; S=4; A.R=0.5; S.R=1.0

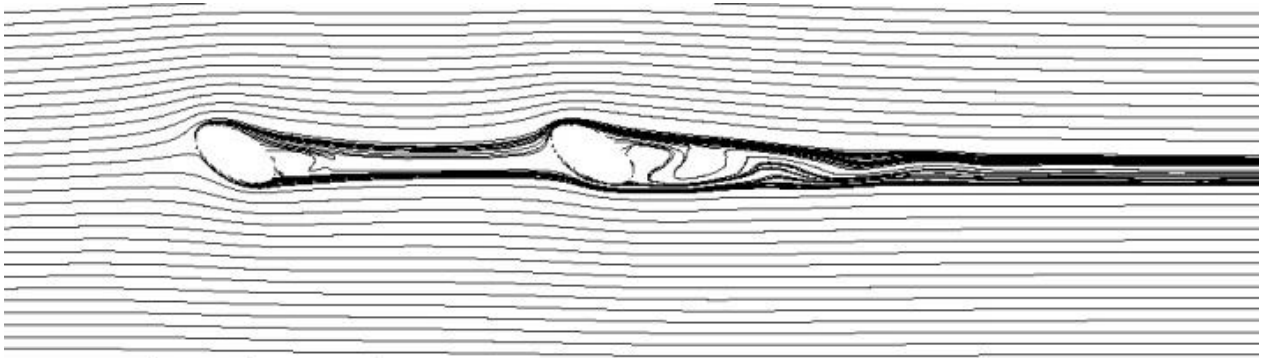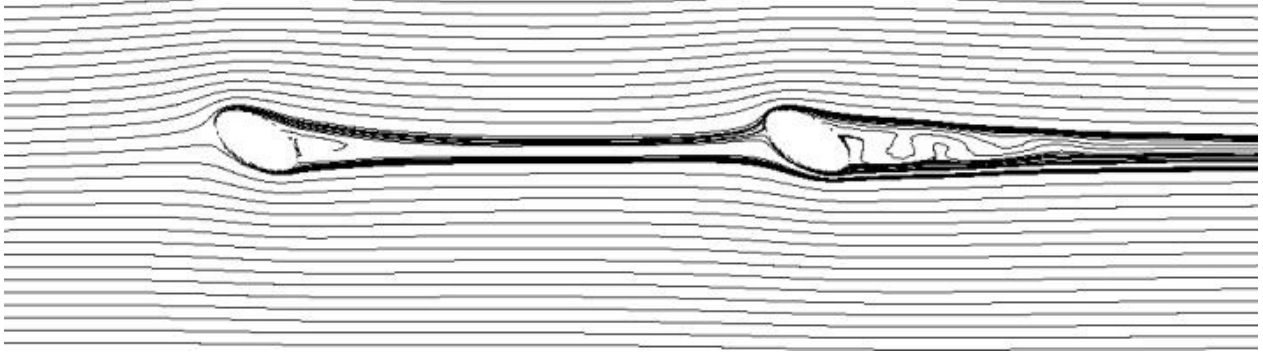**Figure 5.1.4.b:** α=30°; S=6; A.R=0.5; S.R=1.0

At α=30°, S=4 and S=6 streamlines clearly show boundary layer separation as the fluid impinges on leading edge of upstream elliptic cylinders. Shear layers get detached from both upstream cylinders at S=4 and 6. Layer from leading edge has more velocity than the layer at trailing edge. This slip between fluid stream leads to formation of small vortex near trailing edge of both upstream cylinders which creates a zone of low pressure causing drag on the cylinders. Moreover, the wake width at narrowest point of wake is 22% greater for S=4 as compared to S=6. The greater wake width causes lower drag. So the drag at S=4 is lower than at S=6 in experimental study. This can also be seen in the surface plots of upstream cylinder. Now the downstream cylinder experiences wake at its leading edge. Upper shear layer from upstream cylinder glides over both the leading and trailing edges of the downstream cylinder at S=4, whereas the lower shear layer doesnot fully impinge on downstream cylinder at S=6. This recirculation wake can be ascribed to the high pressure region in front of downstream cylinder and low pressure region behind the upstream cylinder. Shear layers separation and small vortex formation is clearly observed for downstream cylinders. But the wake width at upstream of these cylinders (22% greater for S=4 as compared to S=6) contribute to higher drag at S=6 than S=4. This is also evident from surface plots for downstream cylinders.

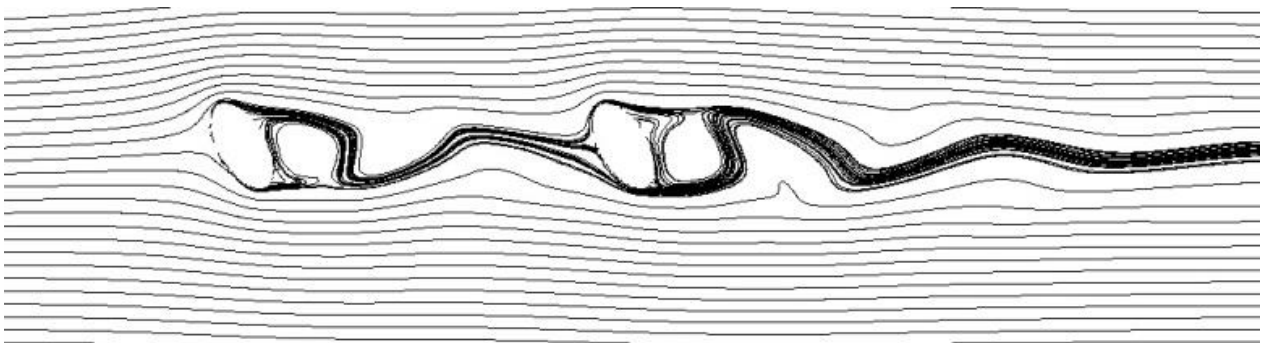**Figure 5.1.5.a:** α=60°; S=4; A.R=0.5; S.R=1.0

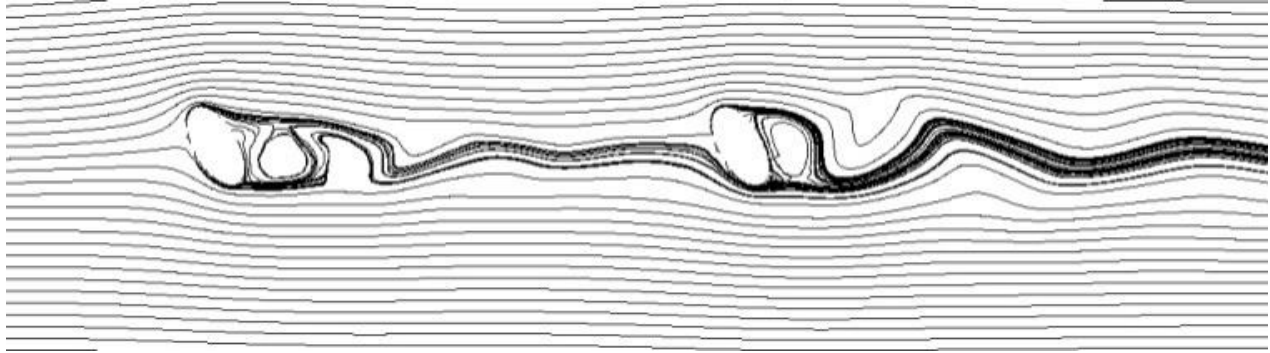**Figure 5.1.5.b:** α=60°; S=6; A.R=0.5; S.R=1.0

At α=60°, S=4 and S=6 streamlines clearly show boundary layer separation as the fluid impinges on leading edge of upstream elliptic cylinders. Shear layers get detached from both upstream cylinders at S=4 and 6. Layer from leading edge has more velocity than the layer at trailing edge. This slip between fluid stream leads to formation of large vortex near trailing edge of both upstream cylinders which creates a zone of low pressure causing drag on the cylinders. The vortex diameter at S=6 is 10% larger than the vortex diameter at S=4. This larger sized vortex cause larger drag at S-6 than S=4. This can also be seen in the surface plots of upstream cylinder. Now the wake of upstream cylinder moves towards front stagnation point of downstream cylinder and detachment of shear layers and large vortex formation can be clearly seen in streamline plots. The vortex diameter at S=6 is 8% larger than vortex diameter at S=4. This large sized vortex causes larger drag at S=6 than S=4. This is also evident from surface plots for downstream cylinders. It is also noteworthy that as the AOA is increased from 0° to 60°, the cylinder apparently changes from slender body parallel to flow to bluff body which intuitively signals increase in drag. This is also evident in surface plots of downstream cylinders.

5.2. Results of Experiments 13 ~ 21
9 experiments were performed at **R$_e$ 14000** and following parameters were used for cylinders. Upstream elliptic cylinder a= 75mm, b= 37.5mm, A.R= 0.5, S.R= 0.5 and downstream elliptic cylinder a= 37.5mm, b= 18.75mm, A.R=0.5, **S.R= 0.5**.

Figure 5.2.1.a: Experimental C_d Upstream Cylinder a= 75mm, b= 37.5mm, A.R= 0.5 & S.R=0.5

Figure 5.2.1.b: Numerical C_d Upstream Cylinder a= 75mm, b= 37.5mm, A.R= 0.5 & S.R=0.5
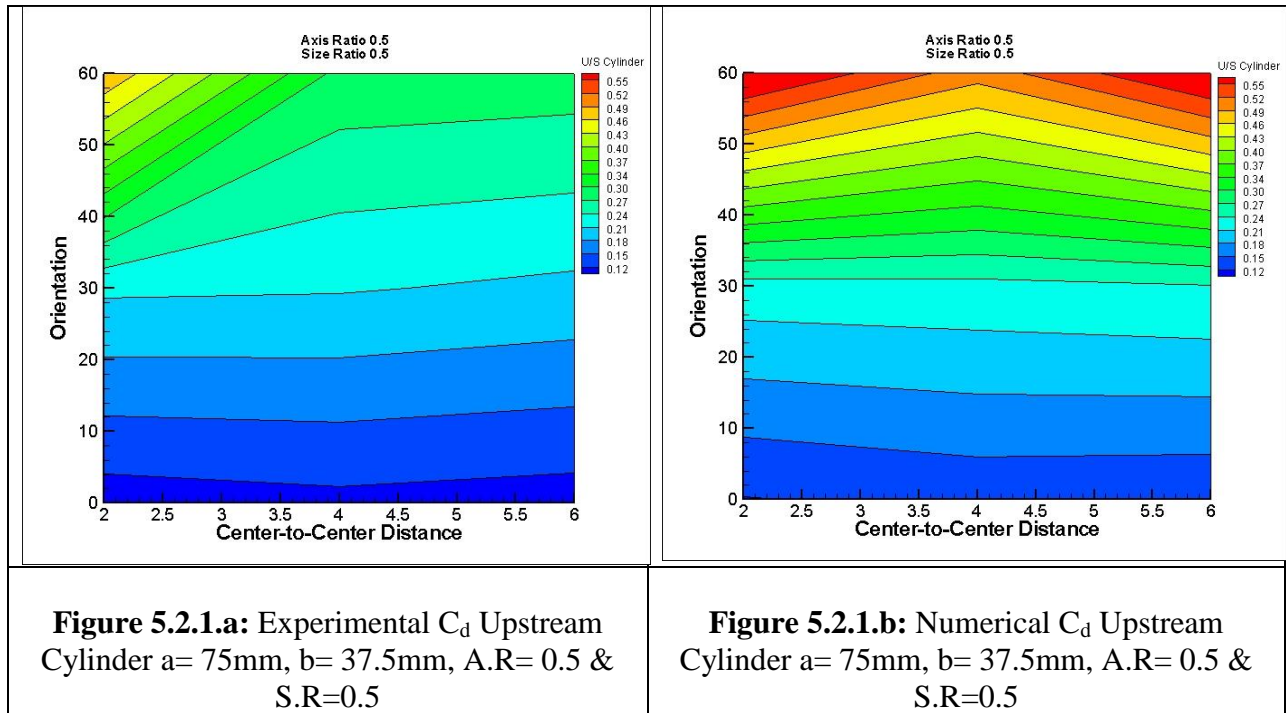
There is not much notable change in coefficient of drag (C_d) with increase in the center-to-center distance (S) for both experimental and numerical study.

However, the general trend of coefficient of drag (C_d) for this case is to increase with orientation (α). When α increases from 0° ~ 30°, C_d increases from 0.12 ~ 0.24 for experimental and 0.15 ~ 0.27 for numerical study. But as α increases from 30° ~ 60°, experimental study although shows a general trend of increase in C_d but shows highest drag at small center-to-center distance (S) of 2, for which drag increases from 0.24 ~ 0.49 but numerical study shows highest drag at center-to-center distance (S) of 2 and 6 , for which drag increases from 0.3 ~ 0.55. C_d increases for center-to-center distance (S) of 4 as well but not as much as the aforementioned case.

| **Figure 5.2.2.a:** Experimental C_d Downstream Cylinder a= 37.5mm, b= 18.75mm, A.R= 0.5 & S.R=0.5 | **Figure 5.2.2.b:** Numerical C_d Downstream Cylinder a= 37.5mm, b= 18.75mm, A.R= 0.5 & S.R=0.5 |
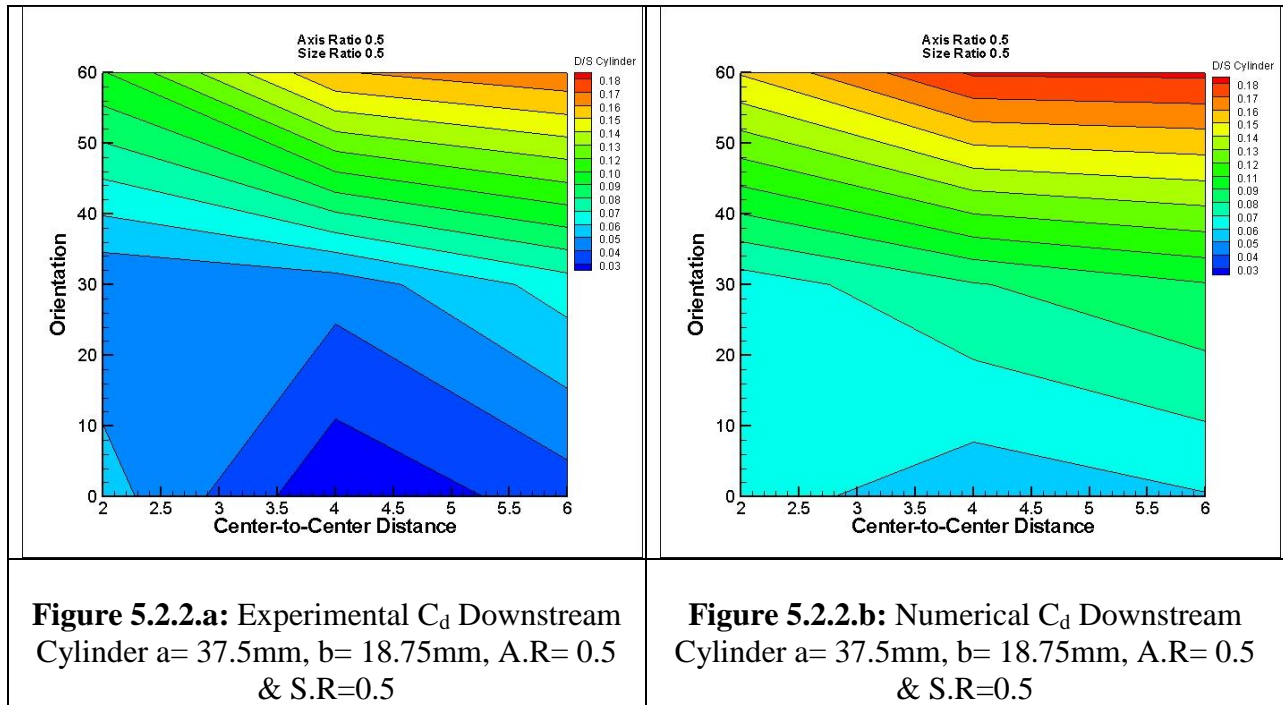
Coefficient of drag (C_d) initially reduces with increase in center-to-center distance (S) upto 4 and then start to increase with further increase in center-to-center distance (S) for both experimental and numerical studies.

Coefficient of drag (C_d) increases with increase in orientation (α) with maximum C_d occurring at 60° orientation and center-to-center distance (S) 6 for both experimental and numerical studies.
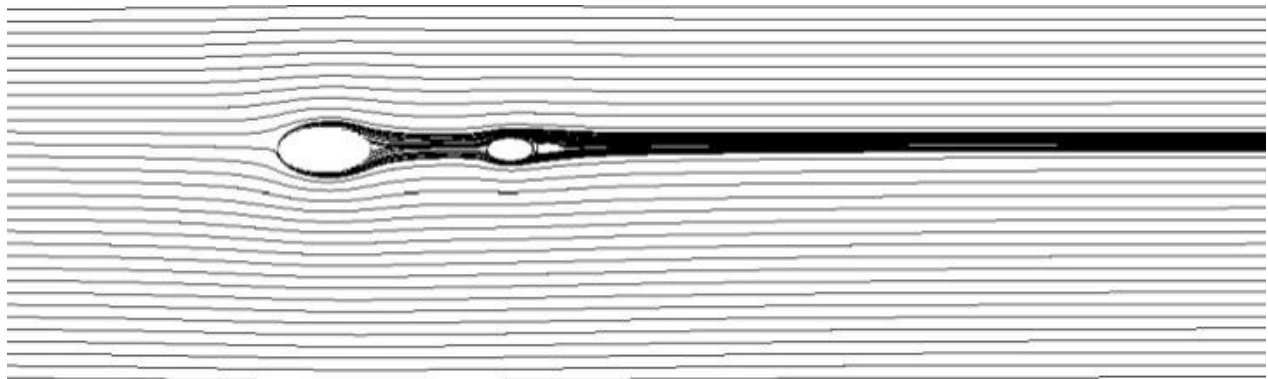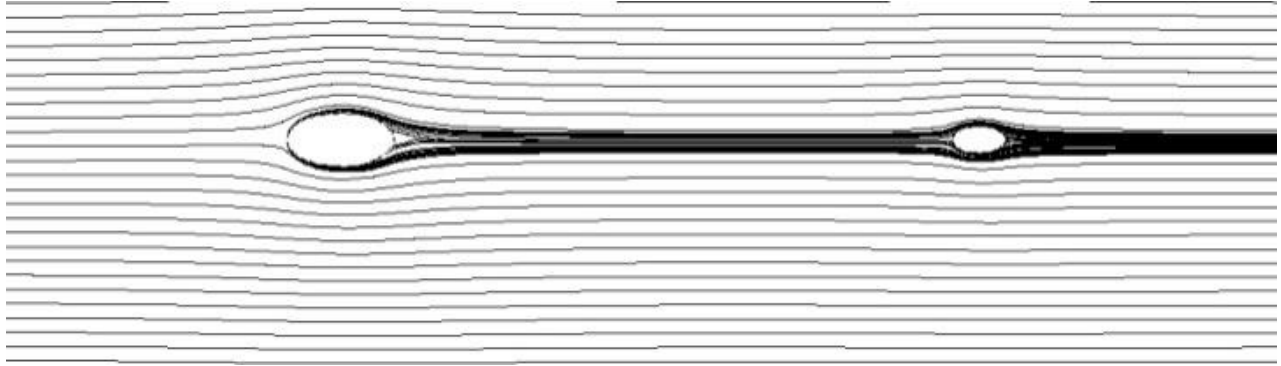

Figure 5.2.3.a: α=0°; S=2; A.R= 0.5; S.R=0.5

Figure 5.2.3.b: α=0°; S=6; A.R= 0.5; S.R=0.5

At α=0°, S=2 and S=6 streamlines clearly show boundary layer separation as the fluid flows around upstream elliptic cylinders. Shear layers get detached from both upstream cylinders at S=2 and 6. Therefore at back stagnation point the pressure is lower than front stagnation point. This low pressure cause drag on upstream cylinders. However the similar streamline behavior leads to the conclusion that C_d of both cylinders will remain same at S=2 and 6. This can also be seen in upstream cylinder surface plots. Now the downstream cylinders experience wake at its leading edge. This recirculation wake can be ascribed to the high pressure region in front of downstream cylinder and low pressure region behind the upstream cylinder. Shear layers separation is clearly visible at trailing edge of downstream cylinders as well and shear layers separation at S=2 is more than the shear layer separation at S=6. Higher shear layer separation causes lower pressure at trailing edge of downstream cylinders which leads to higher drag at S=2 than at S=6. Moreover it can be inferred from the streamline plots that because of lower S.R ($a_{Downstream\ Cylinder}$ / $a_{Upstream\ Cylinder}$ =0.5) the upstream cylinder tends to block the incoming flow of downstream cylinder. So the C_d of downstream cylinder decreases upto S=4 but as S increases to 6 C_d again increases.
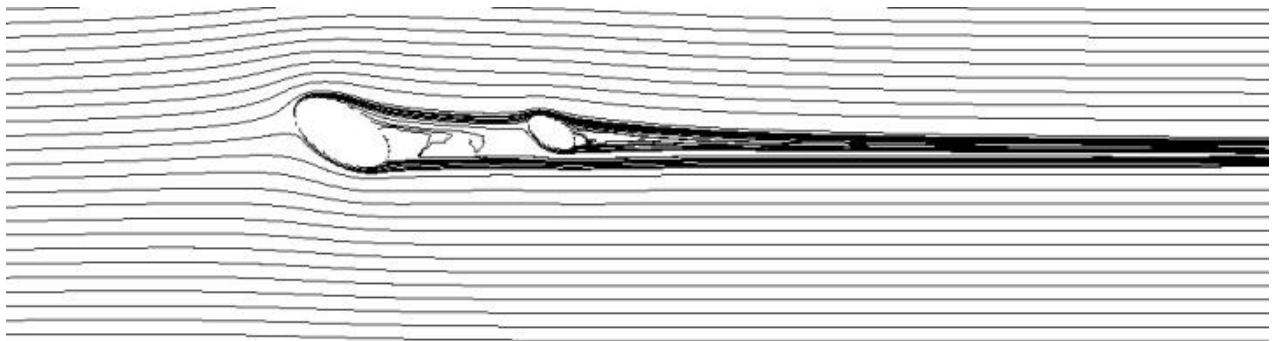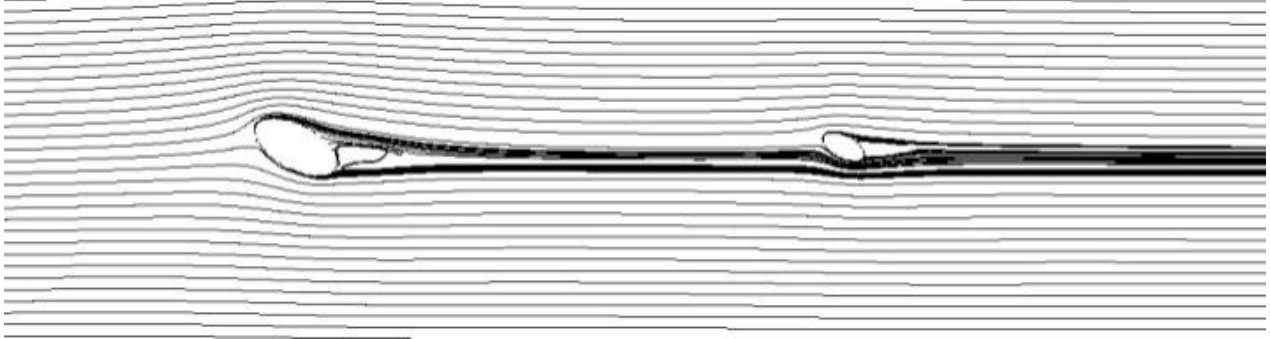

Figure 5.2.4.a: α=30°; S=2; A.R= 0.5; S.R=0.5

Figure 5.2.4.b: α=30°; S=6; A.R= 0.5; S.R=0.5

At α=30°, S=2 and S=6 streamlines clearly show boundary layer separation as the fluid impinges on leading edge of upstream elliptic cylinders. Shear layers get detached from both upstream cylinders at S=2 and 6. Layer from leading edge has more velocity than the layer at trailing edge. This slip between fluid stream leads to formation of small vortex near trailing edge of both upstream cylinders which creates a zone of low pressure causing drag on the cylinders. Similar sized vortex causes almost same drag on both the upstream cylinders. This can also be seen in the surface plots of upstream cylinder. Now the downstream cylinder experiences wake at its leading edge. On one hand, for S=2, Upper shear layer from upstream cylinder glides over both the leading and trailing edges of the downstream cylinder, whereas the lower shear layer doesnot fully impinge on downstream cylinder. This recirculation wake can be ascribed as the high pressure region in front of downstream cylinder and low pressure region behind the upstream cylinder. Shear layers separation and small vortex formation is clearly observed for downstream cylinder. On the other hand, for S=6, upper shear layer gently glides under trailing edge of downstream cylinder and lower shear layer doesnot interact and continues flowing along its original path. But the wake width at upstream of these cylinders, 57% greater for S=2 as compared to S=6 (greater wake width causes lower drag), contribute to lower drag at S=2 than S=6. This is also evident from surface plots for downstream cylinders.
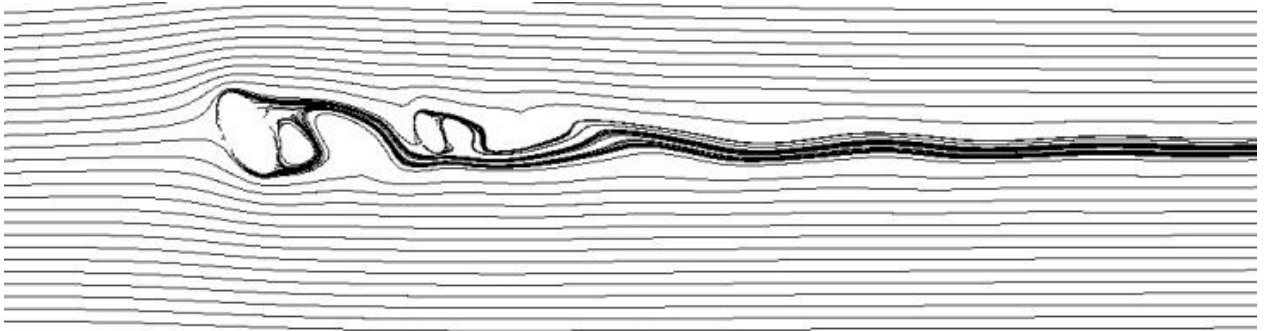

Figure 5.2.5.a: α=60°; S=2; A.R= 0.5; S.R=0.5

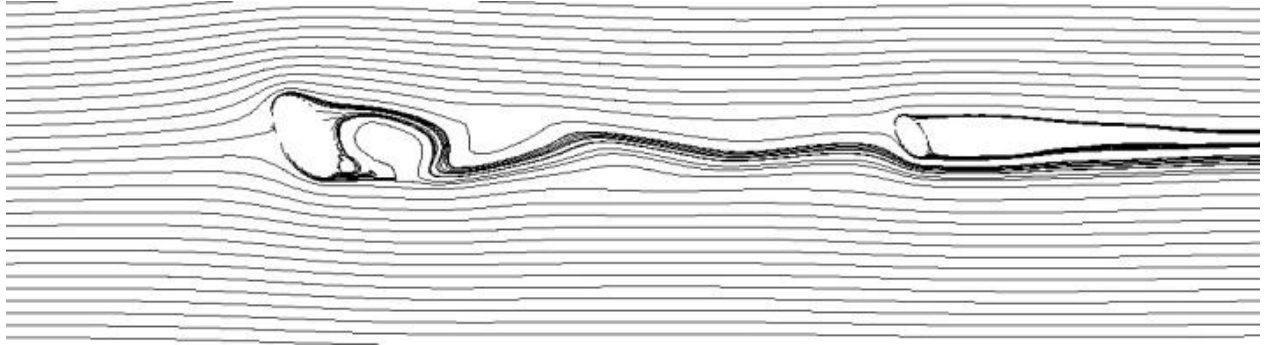**Figure 5.2.5.b:** α=60°; S=6; A.R= 0.5; S.R=0.5

At α=60°, S=2 and S=6 streamlines clearly show boundary layer separation as the fluid impinges on leading edge of upstream elliptic cylinders. Shear layers get detached from both upstream cylinders at S=2 and 6. Layer from leading edge has more velocity than the layer at trailing edge. This slip between fluid stream leads to formation of large vortex near trailing edge of both upstream cylinders. However at S=6, 1 vortex about 10% larger than at S=2 was formed. Whereas, for S=2, 1 large vortex of fairly large size was formed and streamlines tended to form another vortex at S=2. This caused larger C_d at S=2. This can also be seen in the surface plots of upstream cylinder. Now for S=2, the wake of upstream cylinder moves towards front stagnation point of downstream cylinder and detachment of shear layers and large vortex formation can be clearly seen in streamline plots. Whereas, for S=6 a very large and elongated separation can be seen at trailing edger of downstream cylinder. This separation caused larger C_d at S=6 than S=2. This is also evident from surface plots for downstream cylinders. It is also noteworthy that as the AOA is increased from 0° to 60°, the cylinder apparently changes from slender body parallel to flow to bluff body which intuitively signals increase in drag. This is also evident in surface plots of downstream cylinders.

5.3. Results of Experiments 22 ~ 30
9 experiments were performed at **R$_e$ 7000** and following parameters were used for cylinders. Upstream elliptic cylinder a= 37.5mm, b= 18.75mm, A.R= 0.5, S.R= 1.0 and downstream elliptic cylinder a= 37.5mm, b= 18.75mm, A.R=0.5, **S.R= 1.0**.

Figure 5.3.1.a: Experimental C_d Upstream Cylinder a= 37.5mm, b= 18.75mm, A.R= 0.5 & S.R= 1.0

Figure 5.3.1.b: Numerical C_d Upstream Cylinder a= 37.5mm, b= 18.75mm, A.R= 0.5 & S.R= 1.0
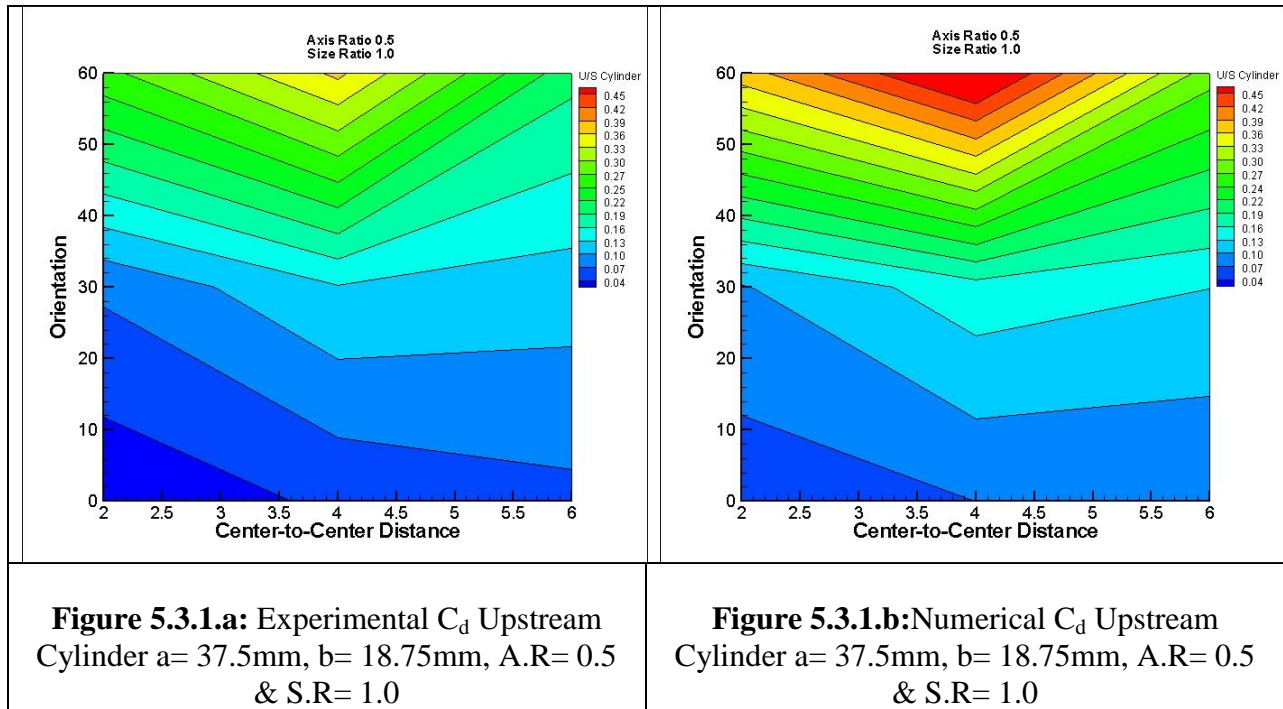
Coefficient of drag (C_d) slightly increases with increase of center-to-center distance (S) for both experimental and numerical study.

However, coefficient of drag C_d shows more dependence on orientation (α). As α increase, C_d increases and reaches its maximum value for 60° and center-to-center distance (S) 4 in both experimental and numerical study. But maximum value of C_d for experimental (0.36) is a bit lower than that predicted by numerical study (0.45).

Figure 5.3.2.a: Experimental C_d Downstream

Figure 5.3.2.b: Numerical C_d Downstream

24
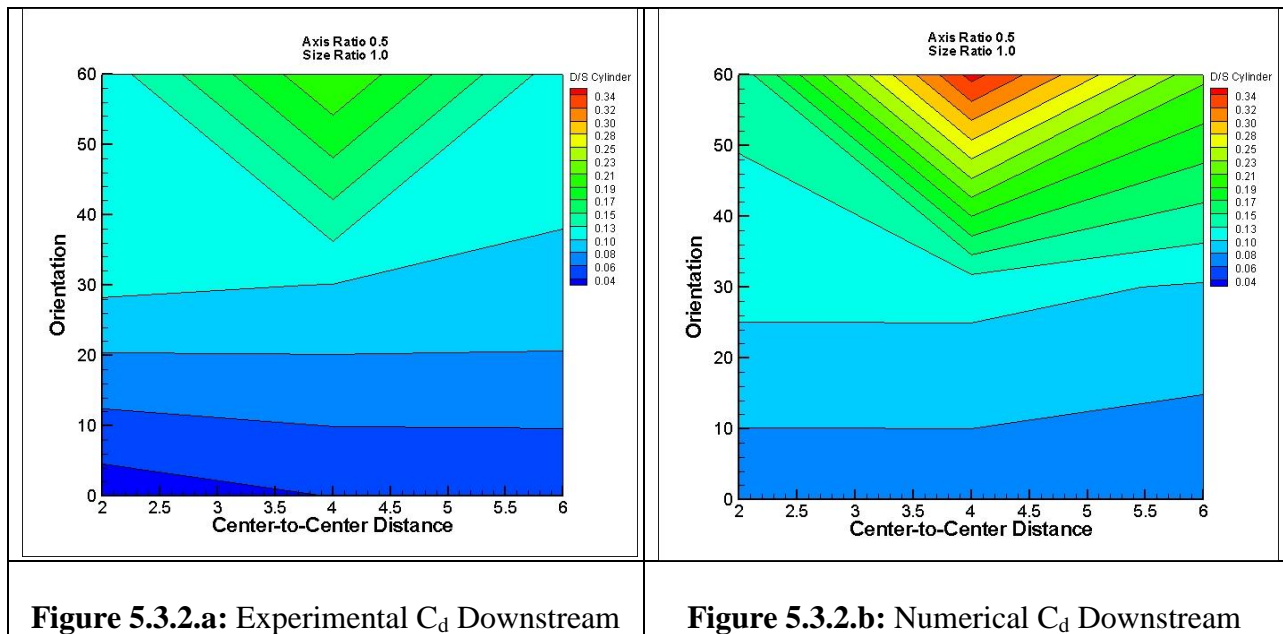
Cylinder a= 37.5mm, b= 18.75mm, A.R= 0.5 & S.R= 1.0	Cylinder a= 37.5mm, b= 18.75mm, A.R= 0.5 & S.R= 1.0

Coefficient of drag (C_d) does not change much with center-to-center distance (S) and remains lowest around 0.06 for experimental study and 0.08 for numerical study.

Although C_d increase for 60° and center-to-center distance (S)2 and 6 but not as much as at 4. C_d reaches its maximum value 0.25 for experimental study and 0.34 for numerical study at 600 and center-to-center distance (S) 4.
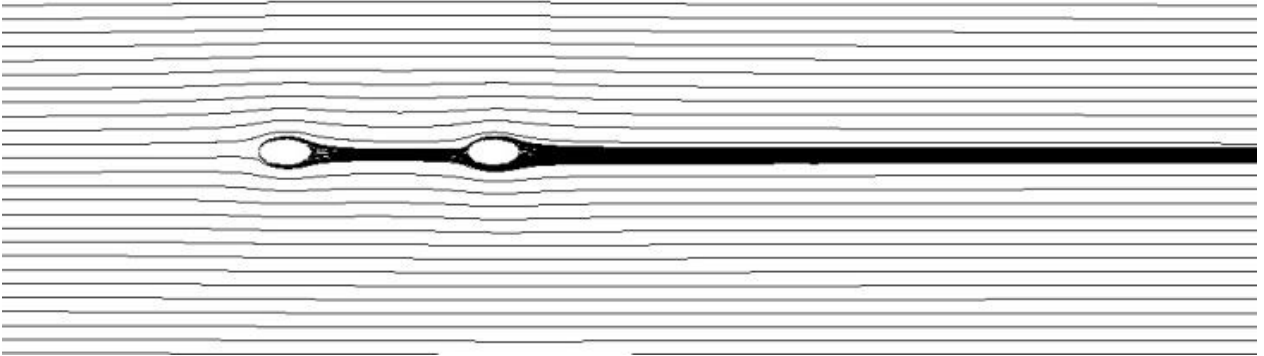
Figure 5.3.3.a: α=0°; S=4; A.R= 0.5; S.R= 1.0
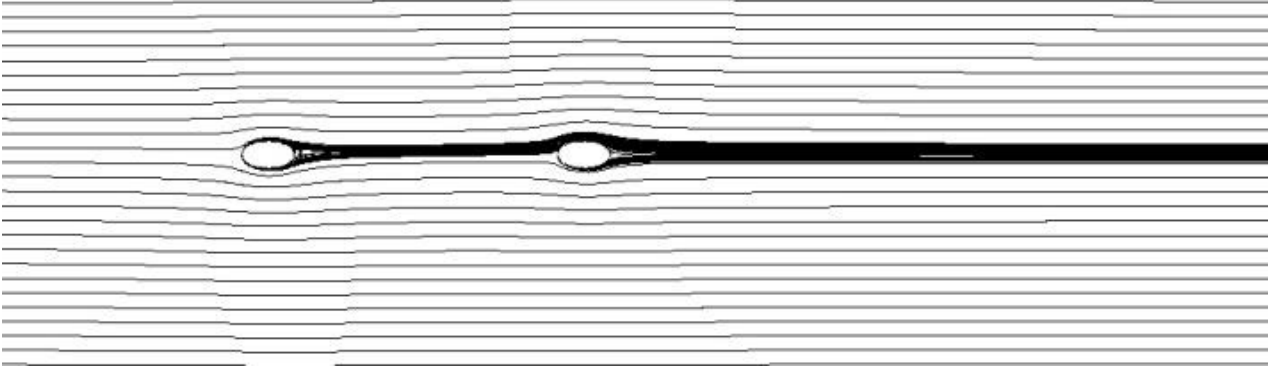
Figure 5.3.3.b: α=0°; S=6; A.R= 0.5; S.R= 1.0

At α=0°, S=4 and S=6 streamlines clearly show boundary layer separation as the fluid flows around upstream elliptic cylinders. Shear layers get detached from both upstream cylinders at S=4 and 6. Therefore at back stagnation point the pressure is lower than front stagnation point. This low pressure cause drag on upstream cylinders. However the similar streamline behavior leads to the conclusion that C_d of both upstream cylinders will remain same at S=4 and 6. This can also be seen in upstream cylinder surface plots. Now the downstream cylinders experience wake at its leading edge. This recirculation wake can be ascribed to the high pressure region in front of downstream cylinder and low pressure region behind the upstream cylinder. Shear layers

separation is clearly visible at trailing edge of downstream cylinders as well. However the similar streamline behavior leads to the conclusion that C_d of both downstream cylinders will remain same at S=4 and 6. This can be seen in surface plots of downstream cylinder.

Figure 5.3.4.a: α=30°; S=4; A.R= 0.5; S.R= 1.0

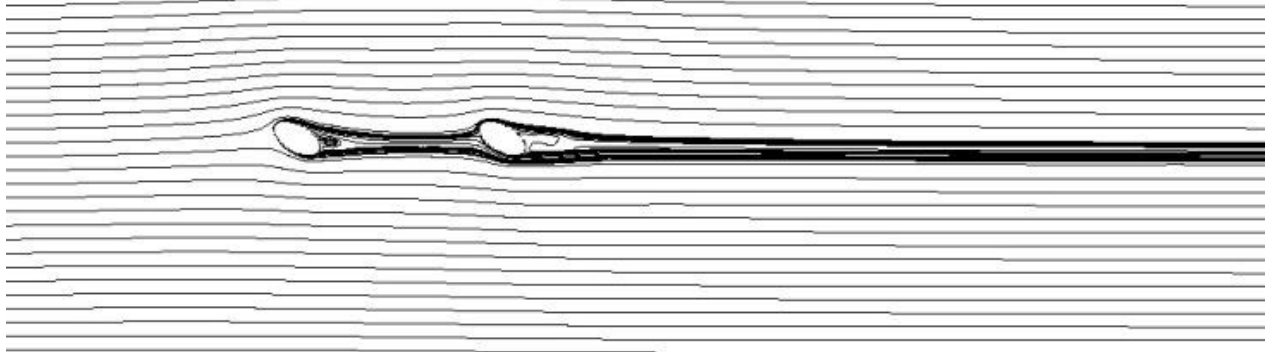**Figure 5.3.4.b:** α=30°; S=6; A.R= 0.5; S.R= 1.0

At α=30°, S=4 and S=6 streamlines clearly show boundary layer separation as the fluid impinges on leading edge of upstream elliptic cylinders. Shear layers get detached from both upstream cylinders at S=4 and 6. Layer from leading edge has more velocity than the layer at trailing edge. This slip between fluid stream leads to formation of small vortex near trailing edge of both upstream cylinders which creates a zone of low pressure causing drag on the cylinders. Because of similar small sized vortex the C_d of both upstream cylinders remain fairly close in value. This can also be seen in surface plots of upstream cylinder. Now the downstream cylinder experiences wake at its leading edge. Upper shear layer from upstream cylinder glides over the leading and lower shear layer from upstream cylinder glides over the trailing edges of the downstream cylinder. This recirculation wake can be ascribed to the high pressure region in front of downstream cylinder and low pressure region behind the upstream cylinder. Shear layers separation and small vortex formation is clearly observed for downstream cylinders. However similar streamline behavior indicates that the C_d of both downstream cylinders will remain same at S=4 and 6. This can be seen in surface plots of downstream cylinders.
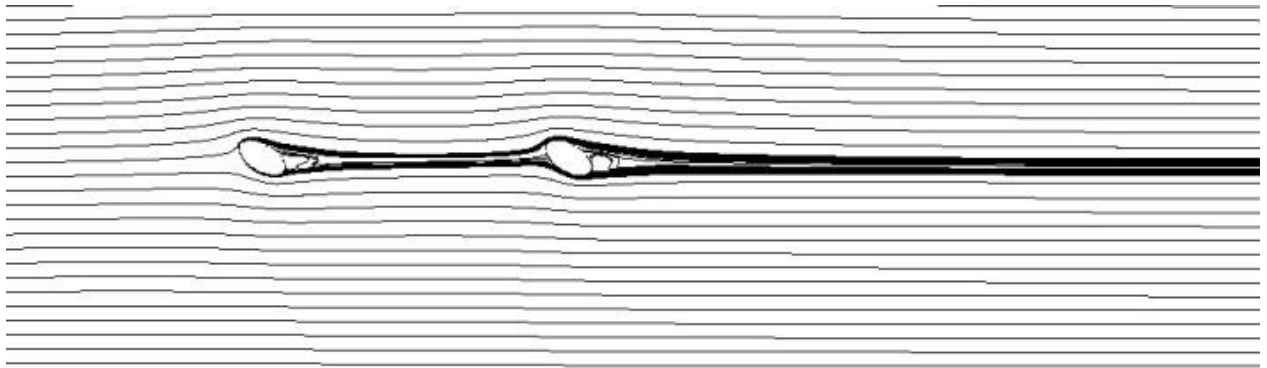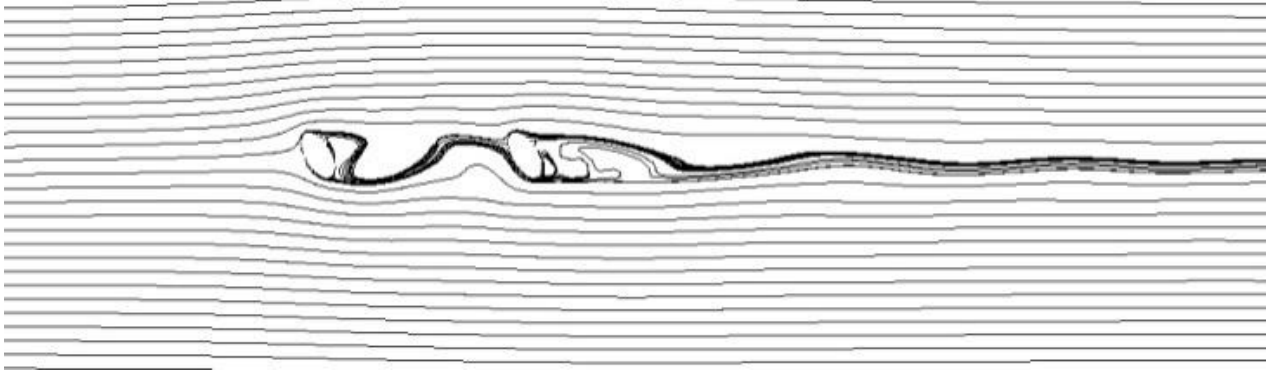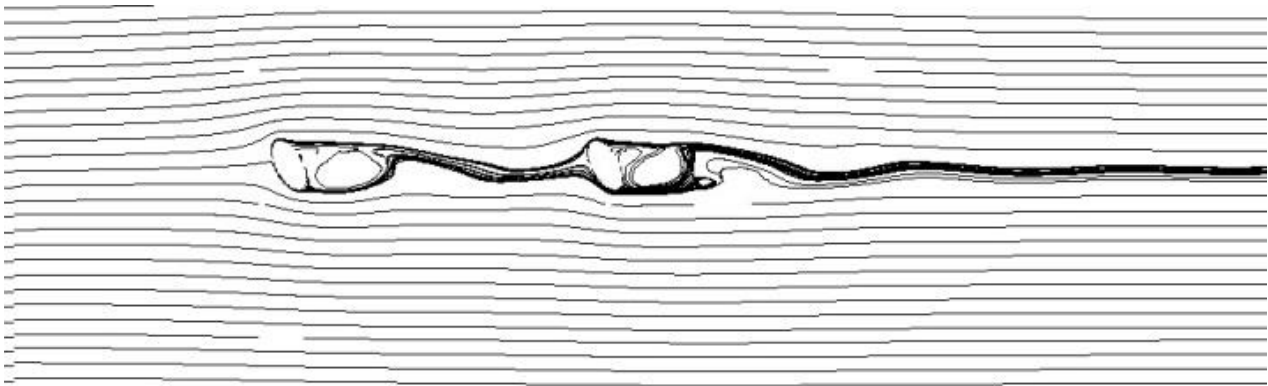
26

Figure 5.3.5.a: α=60°; S=4; A.R= 0.5; S.R= 1.0

Figure 5.3.5.b: α=60°; S=6; A.R= 0.5; S.R= 1.0

At α=60°, S=4 and S=6 streamlines clearly show boundary layer separation as the fluid impinges on leading edge of upstream elliptic cylinders. Shear layers get detached from both upstream cylinders at S=4 and 6. Layer from leading edge has more velocity than the layer at trailing edge. Slip between fluid streamlines generate circulation of fluid which leads to formation of large vortex near trailing edge of both upstream cylinders. This large vortex creates a zone of low pressure causing drag on the cylinders. Moreover the projected area of cylinder is equal at 0° and 30° but when α become 60°, the increase in projected area is 73% (as compared to S=2 and 4) which leads to 194% increase in drag coefficient of upstream cylinders. So the drag at S=4 and α=60° is 194% higher than the drag at S=4 and α=30° for upstream cylinders. This can also be seen in the surface plots of upstream cylinder. Now the wake of upstream cylinder moves towards front stagnation point of downstream cylinder and detachment of shear layers and large vortex formation can be clearly seen in streamline plots. The large vortex causes larger drag on downstream cylinder. Moreover 73% increase in projected area (as compared to S=2 and 4) leads to 104% increase in drag coefficient of downstream cylinder. This is also evident from surface plots for downstream cylinders. It is also noteworthy that as the AOA is increased from 0° to 60°, the cylinder apparently changes from slender body parallel to flow to bluff body which intuitively signals increase in drag. This is also evident in surface plots of downstream cylinders.

27

5.4. Conclusions

1. At R_e 14000, For S.R 1.0, C_d of Upstream and Downstream elliptic cylinders shows dependence on both i.e (S and α) but shows more dependence on orientation than on Center-to Center distance.

2. At R_e 14000, For S.R 0.5 the upstream cylinder experiences greatest C_d at high α and low S. Whereas, for downstream cylinders C_d initially reduces with increase in S and then increases again and the highest C_d occurs at highest α and S.

3. At R_e7000, for S.R 1.0, C_d of Upstream and Downstream elliptic cylinders is maximum at center-to-center distance 4 and orientation (α) 60°.

5.5. Future Recommendations

1. Thorough Numerical and Experimental investigations should be performed for cylinders in parallel arrangement to flow.

2. Flow visualization techniques should be used for better understanding.

3. Apart from study on drag, study on lift coefficient, pressure coefficient and Strouhal Number may also be conducted to verify the relationship between these entities.

Nomenclature

Ø	Diameter of circular cylinder
a	Major Axis of elliptic cylinder
b	Minor Axis of elliptic cylinder
S	Center-to-Center distance between two tandem cylinders
U	Free stream velocity
L	Characteristic length
A	Projected Area or Reference Area
α	Orientation or Angle of Attack (AOA)
ρ	Density
μ	Viscosity
e	Axis Ratio or Aspect Ratio (b/a)
C_d	Coefficient of Drag (2Fd/ρU2A)
R_e	Reynold's Number (ρUL/μ)
S.R	Size Ratio ($a_{\text{Downstream Cylinder}}$ / $a_{\text{Upstream Cylinder}}$)
U/S	Upstream
D/S	Downstream
A.O.A	Angle of Attack

References

[1]   Aref, Hassan, and Eric D. Siggia. "Evolution and breakdown of a vortex street in two dimensions." *Journal of Fluid Mechanics*109 (1981): 435-463.

[2]   Badr, H. M., Dennis, S. C. R., & Kocabiyik, S. (2001). Numerical simulation of the unsteady flow over an elliptic cylinder at different orientations. *International journal for numerical methods in fluids*, *37*(8), 905-931.

[3]   Blevins, R. D. (1977). Flow-induced vibration. *New York, Van Nostrand Reinhold Co., 1977. 377 p.*

[4]   Bokaian, A., & Geoola, F. (1984). Wake-induced galloping of two interfering circular cylinders. *Journal of Fluid Mechanics*, *146*, 383-415.

[5]   Chen, S. S. (1987). *Flow-induced vibration of circular structures*. Hemisphere, Washington, DC.

[6]   Chen, S. S. (1987). A general theory for dynamic instability of tube arrays in crossflow. *Journal of Fluids and Structures*, *1*, 35-53.

[7]   Cimbala, J. M., Nagib, H. M., & Roshko, A. (1988). Large structure in the far wakes of two-dimensional bluff bodies. *Journal of Fluid Mechanics*, *190*, 265-298.

[8]   Fage, A. (1928). I. The flow of air and of an inviscid fluid around an elliptic cylinder and an aerofoil of infinite span, especially in the region of the forward stagnation point. *Phil. Trans. R. Soc. Lond. A*, *227*(647-658), 1-19.

[9]   Faruquee, Z., Ting, D. S., Fartaj, A., Barron, R. M., & Carriveau, R. (2007). The effects of axis ratio on laminar fluid flow around an elliptical cylinder. *International Journal of Heat and Fluid Flow*, *28*(5), 1178-1189.

[10]   Inoue, O., & Yamazaki, T. (1999). Secondary vortex streets in two-dimensional cylinder wakes. *Fluid Dynamics Research*, *25*(1), 1.

[11]   Jackson, C. P. (1987). A finite-element study of the onset of vortex shedding in flow past variously shaped bodies. *Journal of fluid Mechanics*, *182*, 23-45.

[12]   Johnson, S. A., Thompson, M. C., & Hourigan, K. (2001, December). Flow past elliptical cylinders at low Reynolds numbers. In *Proc. 14th Australasian Fluid Mechanics Conference, Adelaide University, South Australia, Dec* (pp. 9-14).

[13]   Johnson, S. A., Thompson, M. C., & Hourigan, K. (2004). Predicted low frequency structures in the wake of elliptical cylinders. *European Journal of Mechanics-B/Fluids*, *23*(1), 229-239.

[14]   Khan, W. A., Culham, J. R., & Yovanovich, M. M. (2005). Fluid flow around and heat transfer from an infinite circular cylinder. *Journal of Heat transfer*, *127*(7), 785-790.

[15]   Kitagawa, T., & Ohta, H. (2008). Numerical investigation on flow around circular cylinders in tandem arrangement at a subcritical Reynolds number. *Journal of Fluids and Structures*, *24*(5), 680-699.

[16]   Mittal, R., & Balachandar, S. (1996). Direct numerical simulation of flow past elliptic cylinders. *Journal of Computational Physics*, *124*(2), 351-367.

[17]   Lugt, H. J., & Haussling, H. J. (1974). Laminar flow past an abruptly accelerated elliptic cylinder at 45 incidence. *Journal of Fluid Mechanics*, *65*(4), 711-734.

[18]   Nair, M. T., & Sengupta, T. K. (1996). Onset of asymmetry: flow past circular and elliptic cylinders. *International Journal for Numerical Methods in Fluids*, *23*(12), 1327-1345.

[19]   Nair, M. T., & Sengupta, T. K. (1997). Unsteady flow past elliptic cylinders. *Journal of fluids and structures*, *11*(6), 555-595.

[20]   Najjar, F. M., & Balachandar, S. (1998). Low-frequency unsteadiness in the wake of a normal flat plate. *Journal of Fluid Mechanics*, *370*, 101-147.

[21]   Paidoussis, M. P. (1980). Flow-induced vibrations in nuclear reactors and heat exchangers. *Practical Experiences and State of Knowledge in Practical Experiences with Flow-Induced Vibrations*, 1-81.

[22]   Paidoussis, M. P. (1981). Fluidelastic vibration of cylinder arrays in axial and cross flow: state of the art. *Journal of Sound and Vibration*, *76*(3), 329-360.

[23]   Paidoussis, M. P. (1983). A review of flow-induced vibrations in reactors and reactor components. *Nuclear Engineering and Design*, *74*(1), 31-60.

[24]   PAIDOUSSIS, M. (1992). Some Curiosity-Driven Research in Fluid Structure Interactions and Current Applications, PVP-1O 1992 Calvin Rice Lecture. In *ASME Winter Annual Meeting 1992*.

[25]   Park, J. K., Park, S. O., & Hyun, J. M. (1989). FLOW REGIMES OF UNSTEADY LAMINAR-FLOW PAST A SLENDER ELLIPTIC CYLINDER AT INCIDENCE. *International Journal of Heat and Fluid Flow*, *10*(4), 311-317.

[26]   Park, J., Kwon, K., & Choi, H. (1998). Numerical solutions of flow past a circular cylinder at Reynolds numbers up to 160. *KSME international Journal*, *12*(6), 1200-1205.

[27]   Patel, V. A. (1981). Flow around the impulsively started elliptic cylinder at various angles of attack. *Computers & Fluids*, *9*(4), 435-462.

[28]   Paul, I., Arul Prakash, K., & Vengadesan, S. (2014). Numerical analysis of laminar fluid flow characteristics past an elliptic cylinder: A parametric study. *International Journal of Numerical Methods for Heat & Fluid Flow*, *24*(7), 1570-1594.

[29]   Taneda, S. (1959). Downstream development of the wakes behind cylinders. *Journal of the physical society of Japan*, *14*(6), 843-848.

[30]   Taneda, S. (1972). The development of the lift of an impulsively started elliptic cylinder at incidence. *Journal of the Physical Society of Japan*, *33*(6), 1706-1711.

[31]   Taneda, S. (1977). Visual study of unsteady separated flows around bodies. *Progress in Aerospace Sciences*, *17*, 287-348.

[32]   Zdravkovich, M. M. (1985). Flow induced oscillations of two interfering circular cylinders. *Journal of Sound and Vibration*, *101*(4), 511-521.

[33]   Zdravkovich, M. M. (1987). The effects of interference between circular cylinders in cross flow. *Journal of fluids and structures*, *1*(2), 239-261.

[34]   Zdravkovich, M. M. (2003). Flow around circular cylinders, vol. 2: applications.

[35]   Zhou, Y., & Alam, M. M. (2016). Wake of two interacting circular cylinders: a review. *International Journal of Heat and Fluid Flow*, *62*, 510-537.